GRK 1782

"Functionalization of Semiconductors"

Seminar 2020

Kloster Höchst, Höchst im Odenwald, 21.09.2020 – 23.09.2020

Research Summaries

supported by: Deutsche Forschungsgemeinschaft

Graduiertenkolleg 1782
“Functionalization of Semiconductors”
Kloster Höchst, Höchst im Odenwald

Seminar Program 21. – 23.09.2020

Monday, 21.09.2020

until 10:30	Arrival
10:30 – 11:00	Coffee Break
	Short Session I Chair: *Luise Rost*
11:00 – 11:30	***Tobias Dunaj***: Synthesis of Interpnictogen Compounds from Diaryl Halido Bismuthanes
11:30 – 12:00	***Alexa Adamkiewicz***: Tip-Induced Surface Reactions Starting from Weakly Bound Intermediates as well as from Covalently Bound Organic Adsorbates on Si(001)
12:00 – 13:00	Lunch
	Session II Chair: *Thilo Hepp*
13:00 – 13:30	***Marcel Kröner***: Growth of Ga(N,As,P)/(B,Ga)(As,P) heterostructures on Si (001) substrate grown with UDMHy and the N-As precursor DTBAA
13:30 – 14:00	***Oliver Maßmeyer***: Decomposition Analysis of TBAs and TBP during GaAs and GaP Growth by MOVPE
14:00 – 14:30	***Johannes Glowatzki***: MOCVD growth studies of GaS monolayers
14:30 – 15:00	Break

15:00 – 17:00 **Postersession**
(including coffee break)

Florian Kreuter: Theoretical investigation of Azulene and Naphtalene on Si(001)-Surface
Fabian Pieck: Automated exploration of reaction networks in chemical vapor deposition by density functional theory
Bertram Peters: Ionothermal Design of Exfoliable Tellurido-mercurate Materials
Christian Ritter*:* Building Interpnictogen Chains
Maximilian Widemann*:* *In-situ* TEM Growth Investigations of III/V Semiconductor Materials
Mikko Wilhelm: Optoelectronic coupling of colloidal quantum dots and semiconductor substrates

17:00 – 18:00 Move into the rooms

18:00 – 19:00 Dinner

Tuesday, 22.09.2020

08:00 – 09:00 Breakfast

Session III Chair: *Alexa Adamkiewicz*

09:00 – 09:30 ***Sven Christian Liebscher***: Extension of the LDA-1/2 method to dilute bismides

09:30 – 10:00 ***Badal Mondal***: Substrate, temperature and pressure effect (strain) on electronic properties of III-V semiconductor from ab-initio approach

10:00 – 10:30 ***Fabian Pieck***: Automated exploration of reaction networks in chemical vapor deposition by density functional theory

10:30 – 11:00 Coffee Break

Short Session IV Chair: *Sven Christian Liebscher*

11:00 – 11:30 ***Luise Rost***: The influence of growth interruption on the luminescence properties of Ga(As,Sb)-based type II heterostructures

11:30 – 12:00 ***Mikko Wilhelm***: Optoelectronic coupling of colloidal quantum dots and semiconductor substrates

12:00 – 13:00 Lunch

13:30 – 17:30 **Discussions**

Networking - Joint nature hike to castle Breuberg

18:00 Dinner

Wednesday, 23.09.2020

08:00 – 09:00	Breakfast
09:00 – 09:30	Tidy up and leave rooms
	Session V Chair: *Oliver Maßmeyer*
09:30 – 10:00	***Johannes Haust***: Analyzing the influence of different growth parameters on the decomposition of MOVPE precursors with mass spectrometry
10:00 – 10:30	***Thilo Hepp****:* Bismuth-containing W type laser structures for long wavelength emission on GaAs substrates
10:30 – 11:00	Coffee Break
11:00 – 11:30	***Robin Günkel****:* In-situ analysis of Ga(N,As)/Ga(As,Bi) interfaces during growth by MOVPE
11:30 – 12:00	Break
12:00 – 13:00	Lunch
afterwards	Departure

Speaker's research summaries

(in order of schedule)

Synthesis of Interpnictogen Compounds from Diaryl Halido Bismuthanes

Tobias Dunaj, Carsten von Hänisch

Department of Chemistry and Material Sciences Center, Philipps-Universität Marburg

Introduction

Di-*tert*-butylarsane amine (DTBAA) can be used as precursor for the synthesis of 13/15-semiconductors via MOCVD methods. Using DTBAA and triethyl gallane, N-doted GaAs-semiconductors can be prepared. In comparison to the established procedure using *tert*-butyl arsane and 1,1-dimethyl hydrazine instead of DTBAA, a higher efficiency for nitrogen incorporation and a lower amount of carbon incorporation can be achieved.[1] In analogy to DTBAA, compounds with the formula $Ar_2Bi\text{-}PnR_2$ (Pn = N-Sb) can be suitable as precursors for the preparation of bismuth and pnioctogen doted semiconductors.

Only few compounds incorporating the structural motif $R_2Bi\text{-}PnR'_2$ (R = Alkyl-, Aryl-; R' = H, Alkyl, Aryl; Pn = N-Sb) are described in the literature.[2-8] By reacting the literature known Mesityl (2,4,6-trimethylphenyl)[9] and phenyl[10], and new Dipp (2,6-Di*iso*propylphenyl) substituted, aryl halido bismuthanes with metalated or silylated pnictogens, we want to build binary interpnictogen compounds bearing, if possibly functionalizable, pnictogen substituents. These binary interpnictogen compounds are tested on their usability as precursors in MOCVD processes. Moreover, further functionalization to ternary and quaternary interpnictogen compounds is attempted.

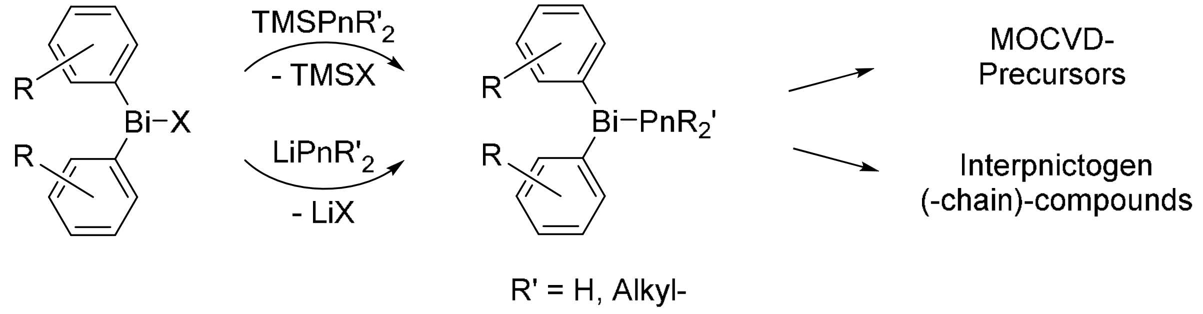

Scheme 1: Aim of the study.

Results

The Dipp substituent was successfully introduced to diaryl bismuth chemistry and compounds of the form $Dipp_2BiX$ (X = F, Cl, Br, I, OTf) were isolated and fully characterized. Reaction of the Mesityl and phenyl, as well as the Dipp substituted diaryl halido bismuthanes with pnictogenides of the form $LiPnR_2$ (Pn = P, As; R = ^{t}Bu, Me) gave binary interpnictogen compounds of the form $Ar_2Bi\text{-}PnR_2$ (**1-3a-c**, scheme 2). Functionalizable amino- or phospha bismuthanes with protons at the pnictogen atoms could not be obtained in pure form using the salt metathesis procedure, although formation of the desired products could be observed spectroscopically in most cases. Using milder reaction conditions, in form of a TMS-X elimination route, phospha bismuthanes with a proton at the phosphorus center were isolated (**2,3d**). Reaction of the dimethylamino bismuthanes and *tert*-butyl amine yielded functionalizable amino bismuthanes through elimination of dimethylamine (**2e**, scheme 2).

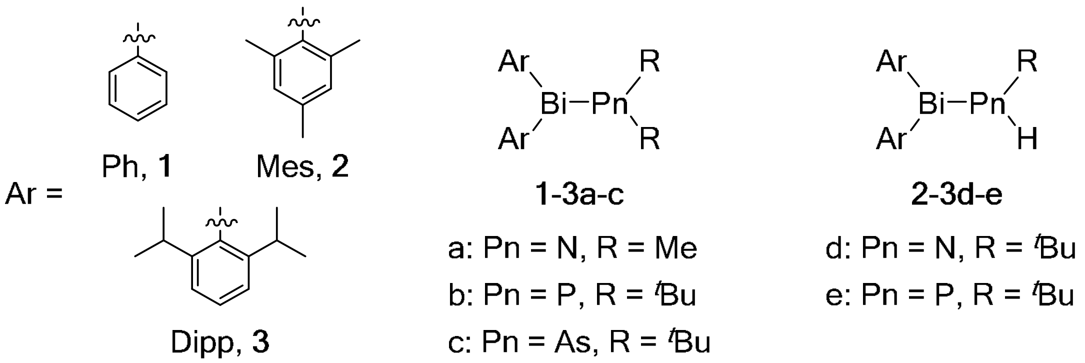

Scheme 2: Prepared Interpnictogen compounds.

Conclusion and Outlook

The obtained binary Interpnictogen compounds might be possible precursors for the use in MOCVD processes. In future experiments the suitability of these compounds as MOCVD precursors will be examined. Moreover, the hydrogen substituted interpnictogen compounds (**1-3d-e**) enable further functionalization of the interpnictogen compounds. This should lead to preparation of ternary or even quaternary interpnictogen compounds. A possible route towards ternary interpnictogen compounds is outlined in scheme 3.

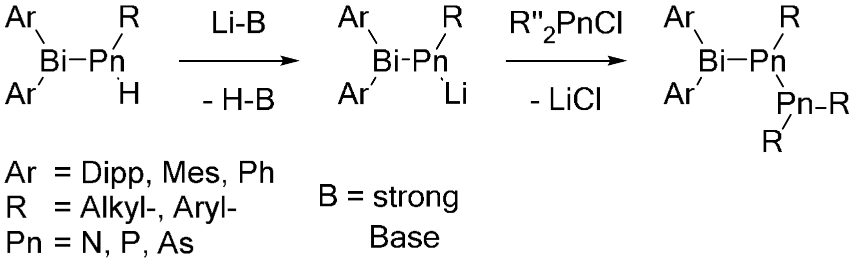

Scheme 3: Possible reaction pathway towards ternary interpnictogen compounds with a terminal diaryl bismuth fragment.

References

[1] C. von Hänisch, W. Stolz, K. Volz, *J. Cryst. Growth* **2016**, *439*, 19-27.

[2] O. J. Scherer, P. Hornig, M. Schmidt, *J. Organomet. Chem.* **1966**, *3*, 259-264.

[3] M. Nieger, G. Schafer, B. Ross, *CSD Commun.*, CCDC 233889 **2004.**

[4] J. W. Wielandt, S. Petrie, N. L. Kilah, A. C. Willis, R. D. Dewhurst, F. Belaj, A. Orthaber, R. Stranger, S. B. Wild, *Aust. J. Chem.* **2016**, *69*, 524.

[5] Y. Matano, H. Nomura, H. Suzuki, M. Shiro, H. Nakano, *J. Am. Chem. Soc.* **2001**, *123*, 10954-10965.

[6] C. Ritter, B. Ringler, F. Dankert, M. Conrad, F. Kraus, C. von Hänisch, *Dalton Trans.* **2019**, *16*, 5253-5262.

[7] A. J. Ashe III, E. G. Ludwig Jr., *J. Organomet. Chem.* **1986**, *303*, 2, 197-204.

[8] H. J. Breunig, D. Müller, *Z. Naturforsch. B* **1986**, *41B,* 9, 1129-1132.

[9] D. H. R. Barton, N. Y. Bhatnagar, J. Flnet, W. B. Motherwell, *Tetrahedron.* **1986**, *42,* 12, 3111-3122.

[10] X. W. Li, J. Lorberth, K. H. Ebert, W. Massa, S. Wocadlo, *J. Organomet. Chem.* **1998**, *2*, 211-215.

Tip-Induced Surface Reactions Starting from Weakly Bound Intermediates as well as from Covalently Bound Organic Adsorbates on Si(001)

Alexa Adamkiewicz[1], Tamam Bohamud[1], Marcel Reutzel[1], Michael Dürr[1,2], and Ulrich Höfer[1]

[1]Department of Physics and Material Sciences Center, Philipps University Marburg, Germany
[2]Institute of Applied Physics, Justus Liebig University Gießen, Germany

Introduction

In order to design and control the functionalization of semiconductor surfaces by means of organic materials, the investigation of the properties of the adsorption process and possible means of manipulating the adsorbates play a crucial role. In particular, organic adsorbates on silicon surfaces are of wide interest as they might serve as an interface between conventional silicon technology and the broad variety of organic functionalities.

Results

Scanning tunneling microscopy and molecular beam studies showed that diethyl ether adsorbs on Si(001) via a datively bound intermediate state[1,2]. Thermal activation (T > 150 K) induces C-O cleavage leading to two covalently bound final states, symmetric (S) and asymmetric (A) (Fig. 1, [1]). In contrast, electronic excitation of the intermediate state was found to lead to a variety of covalently bound final states, which are not obtained by thermal activation[3]. This observation is traced back to a release of the steric restrictions, which apply for the transition state in the case of thermal excitation.

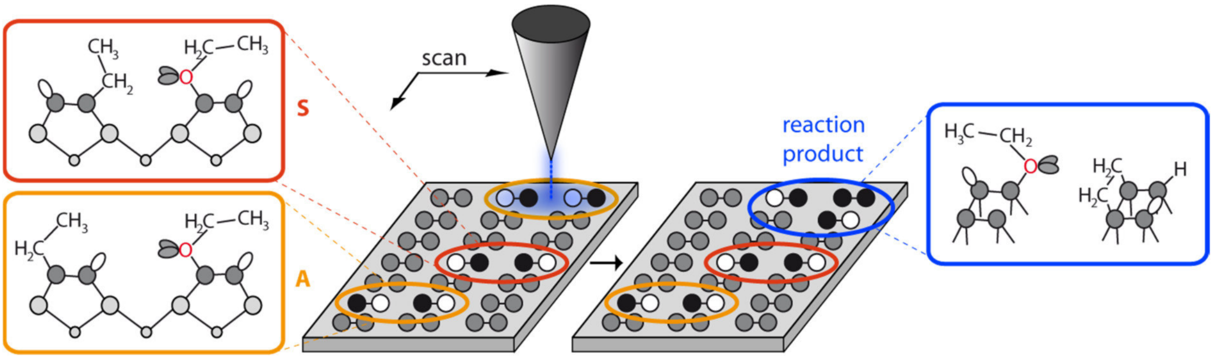

Fig. 1: Scheme representing the two covalently bound adsorption configurations of diethyl ether on Si(001), symmetric (S) and asymmetric (A). Tip-induced excitation enables a surface reaction involving the ethyl species of these configurations. The resulting reaction product extends over three Si dimers.

In addition to this reaction starting from a weakly bound intermediate, tip-induced surface reactions starting from covalently bound molecular configurations were investigated. For this study, the products of the thermally activated ether cleavage of diethyl ether on Si(001) (Fig. 1) served as initial configurations. Applied tunneling bias voltage of above +1.5 V enabled a surface reaction which was restricted to the ethyl species adsorbed on the silicon surface. C-H dissociation at the β carbon atom, followed by the formation of new Si-H and Si-C bonds, led to new products extending over three Si dimers (Fig. 1). At room temperature, the reaction rate depends linearly on the tunneling current, indicating a one-electron excitation process. At 50 K surface temperature, the reaction probability drops significantly, thus thermal activation is additionally necessary for this tip-induced manipulation of covalently bound configurations on the surface[4].

Conclusion

Electronic excitation of surface adsorbate gives access to new reaction products beyond thermal excitation. In this study, we have shown that not only weakly bound intermediate states can be activated in this way but also covalently bound molecular adsorbates can be further manipulated by means of electronic excitation, thus leading the way to more complex reaction schemes and final products.

References

[1] M. Reutzel, G. Mette, P. Stromberger, U. Koert, M. Dürr, and U. Höfer, *J. Phys. Chem. C* **119**, 6018 (2015)
[2] M. Reutzel, M. Lipponer, M. Dürr, and U. Höfer, *J. Phys. Chem. Lett.* **6**, 3971 (2015)
[3] A. Adamkiewicz, T. Bohamud, M. Reutzel, U. Höfer, and M. Dürr, *in preparation*
[4] A. Adamkiewicz, T. Bohamud, M. Reutzel, U. Höfer, and M. Dürr, *in preparation*

Growth of Ga(N,As,P)/(B,Ga)(As,P) heterostructures on Si (001) substrate grown with UDMHy and the N-As precursor DTBAA

M. Kröner[1], P. Ludewig[2], J. Zimmet[2], S. Reinhard[1], C. Ritter[3], C. von Hänisch[3], W. Stolz[1,2]

[1]Department of Physics and Material Sciences Center, Philipps-Universität Marburg
[2]NasP III/V GmbH
[3]Department of Chemistry and Material Sciences Center, Philipps-Universität Marburg

Introduction

One of the big challenges in Si based optoelectronics (OEIC) is the realization of a stable and efficient laser integrated on exact Si (001) substrate. The goal of this project is the pseudomorphical deposition of Ga(N,As,P)/(B,Ga)(As,P)-quantum well heterostructures by metal organic vapour phase epitaxy (MOVPE) with very low defect densities. In order to achieve low defect densities high amounts of N in Ga(N,As,P) are required. Here the use of the novel N-As precursor di-tertiary-butyl-amino-arsane (DTBAA) can be of great use due to its highly superior N incorporation efficiency over the standard N precursor unsymmetrical-di-methyl-hydrazine (UDMHy)[1-3]. Morphological information is obtained by atomic force microscopy (AFM). Optical properties are investigated by photoluminescence spectroscopy (PL), structural and compositional analysis is carried out by means of high resolution X-ray diffraction (HR-XRD).

Results

In order to achieve very low defect densities in Ga(N,As,P) high amounts of N have to be incorporated, since with increasing N content the lattice mismatch of the GaAs based Ga(N,As,P) layer to Si (001) is reduced. For a lattice mismatch of about 2 % to Si (001) we need between 9-10 % N in case of Ga(N,As). The Addition of up to 25 % of P allows for the reduction of the necessary N content down to 4%. Defects that appear during growth can propagate through the overgrown layers, which to a degree makes us able to correlate defect densities in the layer to 3-dimensional platelets on the heterostructures surface. These platelets can be analysed by means of AFM showing the lowest defect densities between 9 and 15 % N[4]. Best structural combined with optical properties using UDMHy are obtained for compositions of Ga(N,As,P) that have about 2 % mismatch. Reducing the mismatch e. g. in Ga(N,As) by further increasing the N content strongly reduces the luminescence intensity (Fig. 1). The necessary N fraction can be achieved using UDMHy for a wide temperature range[5]. However, depending on the desired composition, UDMHy partial pressures of up to 1 mbar can be required for optimized growth conditions due to its low incorporation efficiency, which equals already macroscopic fractions of the overall gas phase of 50 mbar in the reactor during growth. A reduction of the supplied N precursors' partial pressure of DTBAA relative to UDMHy by an order of magnitude can help growing at more well defined conditions and reduce potential carryover of N into overgrown layers that are nominally N-free.

Conclusions & Outlook

The data presented will contain first experiments and a comparison of Ga(N,As,P)/(B,Ga)(As,P) heterostructures grown on exact Si (001) with UDMHy and DTBAA at 525°C growth temperature. Structural as well as optical properties will be compared, in order to be able to judge on advantages and disadvantages of the investigated precursors.

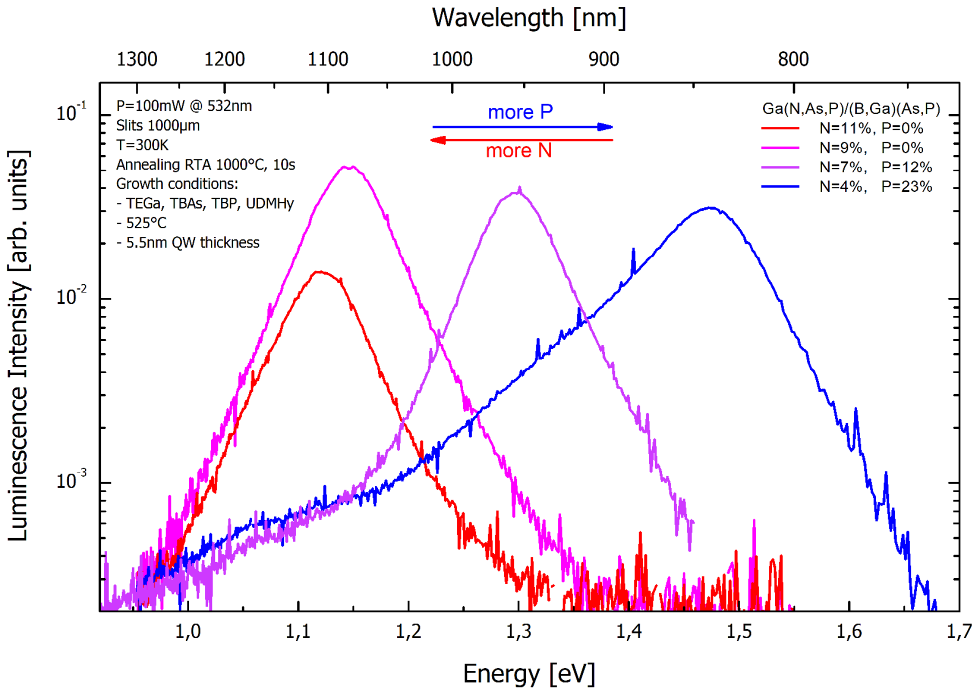

Fig. 1: Room temperature photoluminescence spectra of Ga(N,As,P)/(B,Ga)(As,P) multi quantumwell heterostructures with different compositions at 525°C growth temperature using UDMHy as N precursor.

References

[1] E. Sterzer, A. Beyer, L. Duschek, L. Nattermann, B. Ringler, B. Leube, A. Stegmüller, R. Tonner, C. von Hänisch, W. Stolz, K. Volz, "Efficient nitrogen incorporation in GaAs using novel metal organic As-N precursor di-tertiary-butyl-arsano-amine (DTBAA)", J. Cryst. Growth 439, 19-27 (2016).

[2] E. Sterzer, B. Ringler, L. Nattermann, A. Beyer, C. von Hänisch, W. Stolz, K. Volz, "(GaIn)(NAs) growth using di-tertiary-butyl-arsano-amine (DTBAA)", J. Cryst. Growth 467, 132-136 (2017).

[3] E. Sterzer, O. Maßmeyer, L. Nattermann, K. Jandieri, S. Gupta, A. Beyer, B. Ringler, C. von Hänisch, W. Stolz, K. Volz, "1 eV Ga(NAsSb) grown by MOVPE using di-tertiary-butyl-arsano-amine (DTBAA)", AIP Adv. 8, (2018).

[4] P. Ludewig, M. Diederich, K. Jandieri and W. Stolz, "Growth of high N containing GaNAs/GaP/BGaAsP multi quantum well structures on Si (001) substrates", J. Cryst. Growth 467, 61-64 (2017).

[5] P. Ludewig, S. Reinhard, K. Jandieri, T. Wegele, A. Beyer, L. Tapfer, K. Volz and W. Stolz, "MOVPE growth studies of Ga(NAsP)/(BGa)(AsP) multi quantum well heterostructures (MQWH) for the monolithic integration of laser structures on (001) Si-substrates", J. Cryst. Growth 438, 63-69 (2016).

Decomposition Analysis of TBAs and TBP during GaAs and GaP Growth by MOVPE

O. Maßmeyer, J. Haust, J. Glowatzki, T. Hepp, W. Stolz and K. Volz

Department of Physics and Material Sciences Center, Philipps-Universität Marburg

Introduction

For metal organic vapor phase epitaxy (MOVPE) a thorough understanding of the gas phase reactions and an in-situ gas phase analysis is desired to improve the current understanding of the growth process and improve process control for fabrication of semiconductor devices. Especially, for the deposition of III/V semiconductors highly purified metalorganic precursors are necessary to avoid high defect densities within the structures. Furthermore, small changes in the gas phase mixture can have a significant impact on the growth characteristics[1]. To address these issues we developed a setup for in-situ gas analysis by mass spectrometry used in line in an AIXTRON AIX 200 MOVPE system.

The mass spectrometer is based on a novel fast Fourier transform (FFT) quadrupole ion trap (iTrap) and is attached to the reactor with a bypass. The bypass system is operated under stable flow and pressure conditions to achieve reliable and comparable measurement data. To overcome the large pressure difference between the reactor chamber (50 mbar) and the ion trap (10^{-10} mbar) the analyte is pulsed from the bypass into the mass spectrometer by an atomic layer deposition valve. Due to the FFT based concept, a single mass spectrum can be recorded in less than 2 s and the setup is capable to detect impurities in the parts per trillion level (10^{-12})[3].

Results and Conclusions

In this study this setup was used to investigate the general influence of the Ga precursors trimethylgallium (TMGa), triethylgallium (TEGa) and tritertiarybutylgallium (TTBGa) on the decomposition of tertiarybutylarsane (TBAs) and tertiarybutylphosphane (TBP) during growth of GaAs and GaP, respectively.

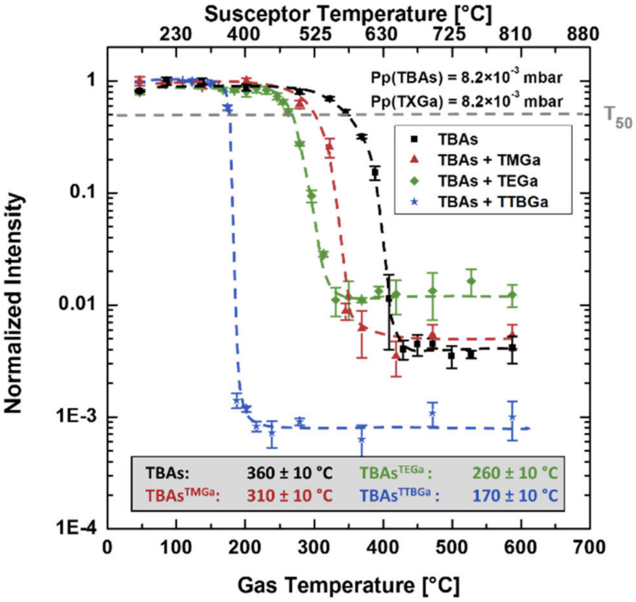

Fig. 1: Decomposition curves of TBAs and during GaAs growth with TMGa, TEGa and TTBGa on the bare susceptor.

The corresponding decomposition curves of TBAs alone (unimolecular decomposition) and during GaAs growth with three different Ga precursors TMGa, TEGa and TTBGa (bimolecular decomposition) are shown in Fig. 1.

From these curves the decomposition temperature of the precursors can be determined by the temperature at which the detected intensities drop to half of their value (dashed gray line). One observes that the decomposition temperature of TBAs is significantly reduced by addition of the Ga precursors. The resulting temperatures are in good agreement with the decomposition temperature for the unimolecular decomposition of the Ga precursors. The strong reduction of the TBAs decomposition temperature down to the one of the Ga precursors indicates a catalytic decomposition process during GaAs growth. Furthermore, the detected reaction products indicate that the alkyl groups of the precursors have to be involved in the decomposition process. Consequently, one underlying reaction is believed to be an alkyl exchange between the Ga precursors and the TBAs, which is schematically shown in reaction 1.

Reaction 1: Illustration of an alkyl exchange reaction.

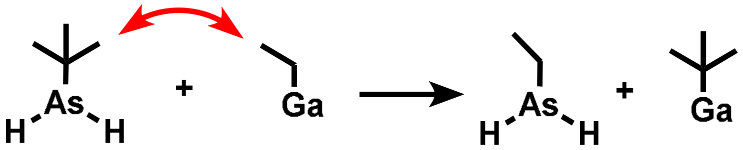

In the subsequent reactions, the alkyl groups are mainly abstracted by homolysis. The homolysis of the tertiary butyl group from TBAs in the presence of the Ga precursor is in contrast to the decomposition of TBAs alone (unimolecular) in which the β-H elimination reaction was shown to be the dominant process at higher temperatures[2,4]. These results including a more in-depth analysis of the detected reaction products and similar findings for GaP growth with TBP and the mentioned Ga precursors will be discussed in more detail in the presentation.

Outlook

In prospective work on this topic, a more detailed investigation of the bimolecular reactions of TBP and the used Ga precursors is planned to improve the understanding of the underlying alkyl exchange reactions. Besides the alkyl exchange more reaction pathways exist, which can be studied for different precursor combinations. For example studies of the bimolecular decomposition of the nitrogen precursor 1,1-dimethylhydrazine (UDMHy) with TMGa or TEGa exhibits adduct formation. Besides the named precursors, many more metal organic precursors are frequently used, which should be investigated in our setup to get more insight on the underlying reactions during epitaxy. Furthermore, a correlation to theoretical calculations of the decomposition reactions is desired in the future.

References

[1] A. Brauers, Prog. Cryst. Growth Charact. Mater. 1991, 22, 1–18.
[2] L. Nattermann, et. al., Sci. Rep. 2018, 8, 1.
[3] H. Y. Chung, et. al., 27th Annu. SEMI Adv. Semicond. Manuf. Conf. ASMC 2016, 263−266.
[4] C. A. Larsen, et. al., J. Cryst. Growth 1989, 94 (3), 663−672.

MOCVD growth studies of GaS monolayers

J. Glowatzki[1], M. Fey[2], T. Hepp[1], O. Maßmeyer[1], S. Chatterjee[2], W. Stolz[1] and K. Volz[1]

[1]Department of Physics and Material Sciences Center, Philipps-Universität Marburg
[2]Institute of Experimental Physics I, Justus-Liebig-Universität Gießen

Introduction

Two dimensional (2D) semiconductors have received great attention due to their extraordinary thickness dependent properties. With graphene there was developed a material with outstanding thermal and electrical properties. Unfortunately, graphene has a band gap of 0 eV but for advanced optical and logical applications semiconducting material is necessary. Typical 2D semiconductors are transition metal dichalcogenides (TMDC), which were studied intensively the last years. A typical behavior for many TMDCs is the band gap decrease with lower thickness and a transition from an indirect band gap to a direct band gap when reaching the monolayer limit[1]. Another class of 2D semiconductors are the layered III-VI semiconductors like GaS, GaSe and InSe, which show a different behavior. The band structure shows a unique Mexican hat shape. This band structure received high attention in the last years, because it is expected to have properties such as unconventional superconductivity and ferromagnetism[2]. Further, 2D GaS and GaSe show a bandgap over 3 eV, which makes them candidates for visible LEDs and also the composition tuning of multilayer GaS_xSe_{1-x} shows bandgaps between 2.0 and 2.5 eV[3]. Many synthesis strategies have been applied through this material class like mechanical exfoliation, ultrasonic exfoliation, powder source based techniques such as chemical vapor deposition (CVD)[4]. Naming the CVD approach good results were achieved in the synthesis of GaS and GaSe in means of single crystal flake size and reaching coalesced monolayers on amorphous substrates like SiO2/Si[3]. Nevertheless, the growth parameters like gas phase compositions can only be changed in a small window and are not well known. Furthermore, the substrate size and the homogeneity of monolayers over the substrates are often unsatisfying[5]. For these reasons the growth of GaS on different amorphous and single crystalline substrates with metal organic precursors in a metal organic chemical vapor deposition (MOCVD) system is investigated systematically and the samples are characterized by means of atomic force microscopy (AFM), scanning electron microscopy (SEM) and Raman spectroscopy.

Results

First growth experiments took place on C-plane (0001) Sapphire substrates with the Ga precursor tritertiarybutylgallium and the S precursor ditertiarybutylsulphide. Different samples were grown at fixed gas phase compositions for 30 min at different temperatures and the nucleation of monolayers and grains occur at decreasing densities for increasing temperature and seem to follow an exponential behavior as seen in Fig. 1a. Also the monolayer diameter and the ratio of monolayer area over grain area are increasing with the temperature (not shown here). As an example for the combination of grain and monolayer an AFM image is shown in Fig. 1b. The monolayers surround the grain in a round shape and sometimes they are coalescing. The height of the monolayer is around 0.8 nm as shown in the line scans in Fig. 1c.

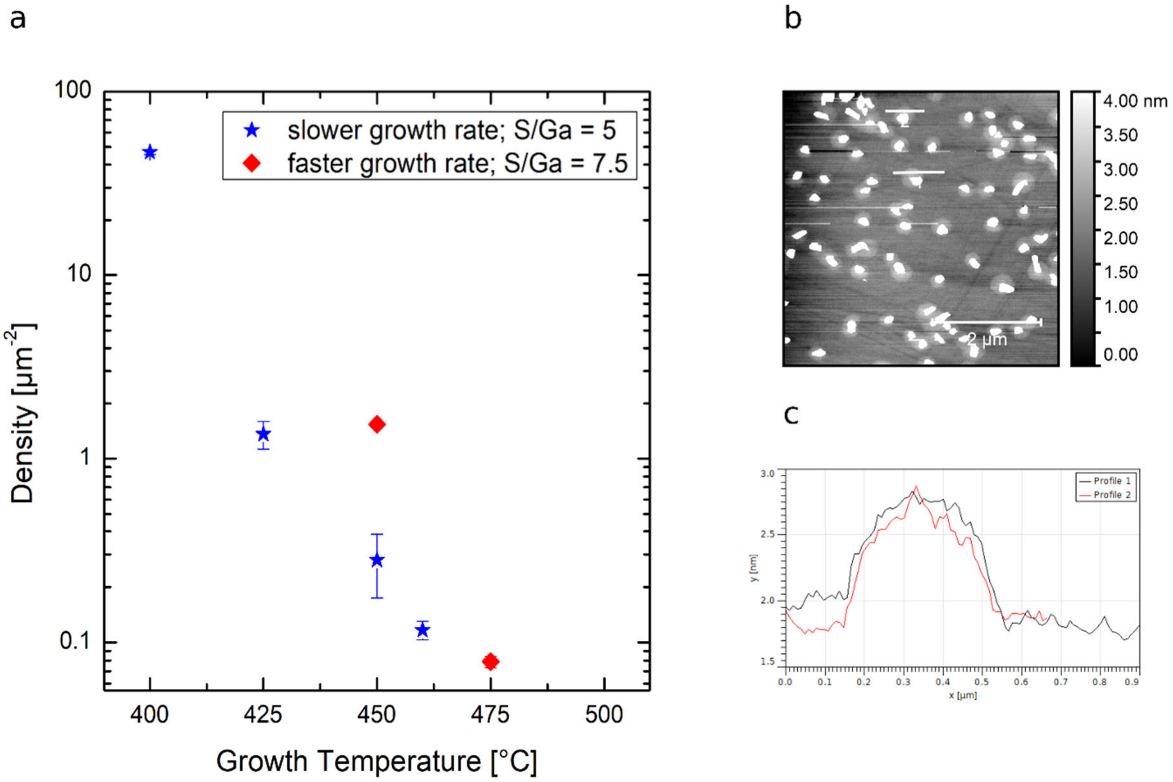

Fig. 1: a shows the density of nucleated grains and monolayers versus the growth temperatures for different gas phase compositions. b shows an exemplary AFM image grown at 450 °C at the faster growth rate out of a and c shows two line scans on two monolayer related regions out of the AFM image in b.

Conclusion and Outlook

Various growth parameters such as S/Ga gas phase ratio, varying total amount of gas, growth time and temperature on sapphire will be investigated systematically and also Raman spectroscopy measurements will be shown and compared to the growth parameters in means of different phases of gallium sulfide like GaS and different types of Ga_2S_3. In addition, growth at different substrates such as GaAs, GaP/Si and soda lime glass will be compared.

References

[1] A. V. Kolobov, J. Tominaga, “Two-Dimensional Transition-Metal Dichalcogenides”, Edition 1, Springer International Publishing, 2016

[2] H. Cai, Y. Gu, Y.-C. Lin, Y. Yu, D. B. Geohegan and K. Xiao, “Synthesis and emerging properties of 2D layered III–VI metal chalcogenides”, Appl. Phys. Rev. 2019, 6, 041312

[3] C. S. Jung, F. Shojaei, K. Park, J. Y. Oh, H. S. Im, D. M. Jang, J. Park and H. S. Kang, “Red-to-Ultraviolet Emission Tuning of Two-Dimensional Gallium Sulfide/Selenide”, ACS Nano 2015, 9, 10, 9585-9593

[4] Y. Lu and J. H. Warner, “Synthesis and Applications of Wide Bandgap 2D Layered Semiconductors Reaching the Green and Blue Wavelengths”, ACS Appl. Electron. Mater. 2020, 2, 7, 1777-1814

[5] X. Wang, Y. Sheng, R.-J. Chang, J. K. Lee, Y. Zhou, S. Li, T. Chen, H. Huang, B. F. Porter, H. Bhaskaran, and J. H. Warner, “Chemical Vapor Deposition Growth of Two-Dimensional Monolayer Gallium Sulfide Crystals Using Hydrogen Reduction of Ga_2S_3”, ACS Omega 2018, 3, 7, 7897-7903

Extension of the LDA-1/2 method to the material class of bismuth containing III-V semiconductors

Sven C. Liebscher[1], Lars C. Bannow[1], Jörg Hader[2], Jerome V. Moloney[2], Stephan W. Koch[1]

[1]Department of Physics and Material Sciences Center, Philipps-Universität Marburg
[2]Wyant College of Optical Sciences, University of Arizona

Introduction

Dilute bismides are promising candidates for applications in opto-electronic devices. Density Functional Theory (DFT) is often used to predict specific opto-electronic material properties. We investigated a way to use the LDA-1/2 (local density approximation minus one half) method within DFT for dilute bismides. This method reduces the computational cost of the calculations, thus allowing for larger simulations with more accurate results. Therefore, the ongoing research on dilute bismides can be facilitated by employing this method.

Results

The LDA-1/2 method[1] adds the so-called 'self-energy potential' to the pseudopotentials used in DFT to improve the predicted bandgaps of solids. In order to construct the LDA-1/2 potential for a specific compound, a cutoff radius that maximizes the bandgap has to be determined. This is not possible for III-Bi semiconductors, because they are semi-metals. Therefore, the cutoff radius of other III-V semiconductors has been extrapolated as a linear function of the covalent radius to approximate the cutoff radius for Bi. Using this cutoff radius, the LDA-1/2 method can be used for dilute bismides.

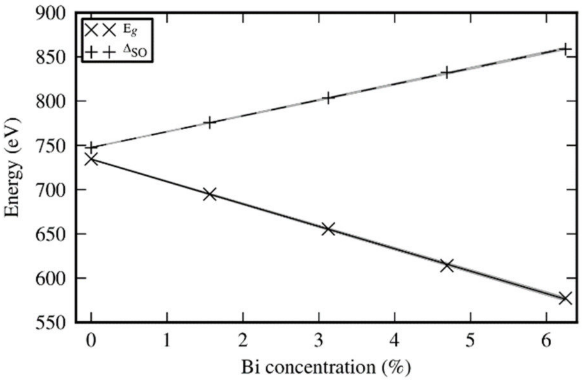

Fig. 1: Bandgap and spin-orbit splitting energies for Ga(SbBi) supercells from DFT calculations with the LDA-1/2 method

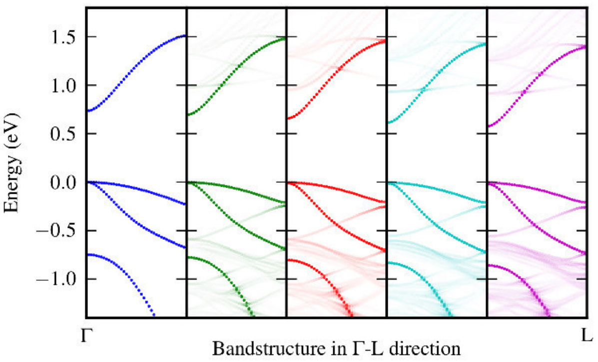

Fig. 1: Effective bandstructures for Ga(SbBi) supercells with increasing Bi concentration f.l.t.r

In order to predict the optoelectronic properties, DFT calculations on Ga(SbBi) supercells consisting of 64 primitive cells have been performed. The incorporation of Bi leads to a bandgap narrowing of 25meV/%Bi and an increase in spin-oribt splitting of 18meV/%Bi, see Fig. 1. The electronic bandstructure of the supercells has been unfolded to obtain the effective bandstructure[2] for different Bi concentrations, see Fig. 2. The conduction bands and the split-off band shift downwards relative to the valence band maximum. Above the conduction band edge and beneath the valence band edge, more and more defect bands emerge for higher concentrations. Furthermore, the splitting between the heavy-hole and light-hole band at the Gamma point increases exponentially.

Using the Semiconductor Bloch Equations[3], the time dynamics of the microscopic polarizations and occupations can be calculated by using the dipole and Coloumb matrix elements from the DFT calculations as input.

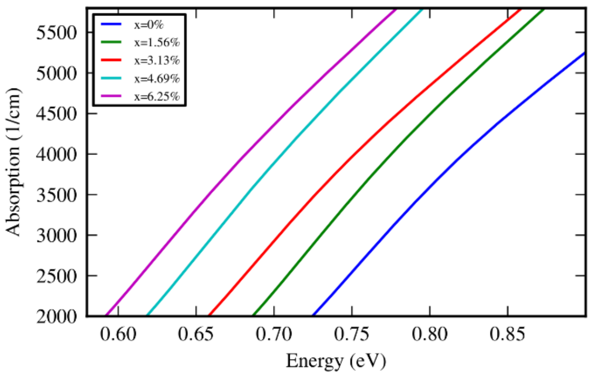

Fig. 2: Absorption spectra of Ga(SbBi) supercells with different Bi concentrations x

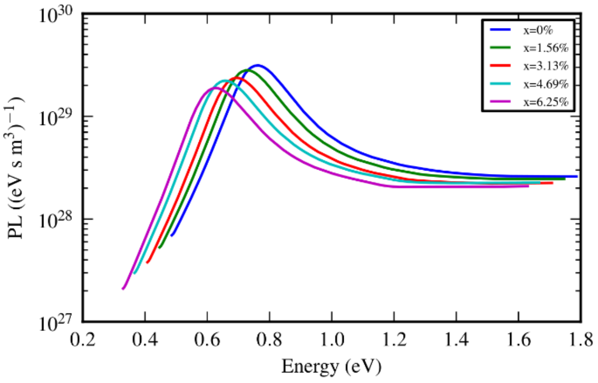

Fig. 4: Photoluminescence spectra of Ga(SbBi) supercells with different Bi concentrations x

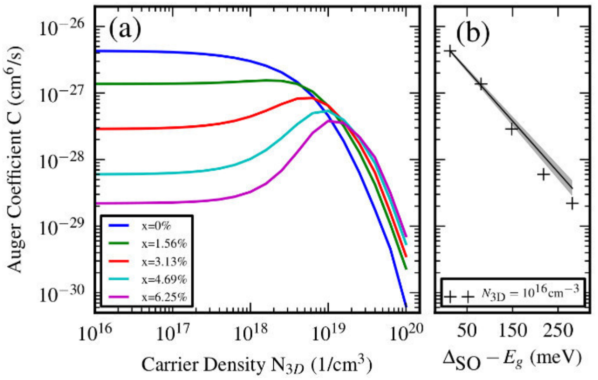

Fig. 5: Auger losses of Ga(SbBi) supercells for different Bi concentrations. (b) Auger losses for low densities as function of the detuning between bandgap and spin-orbit splitting energy

As a result, absorption and luminescence spectra have been calculated, see Figs. 3 and 4. At the respective bandgap energy for every Bi concentration, the absorption increases exponentially and the photoluminescence reaches a maximum.

From the Semiconductor Luminescence Equations[4], the Auger loss coefficient C has been calculated as a function of the carrier density, see Fig. 5. In the low-density regime, the losses decrease exponentially as a function of the detuning between the bandgap and the spin-orbit splitting energy.

For high densities, the losses decrease overall, with higher Bi concentrations yielding higher losses.

Conclusions

The LDA-1/2 method for DFT calculations requires less memory than other exchange-correlation functionals while yielding good results for most semiconductor compounds. Up to date, the LDA-1/2 method could not be used for dilute bismides, because the construction of the LDA-1/2 potential involves maximizing the bandgap of the compound. We introduced a new method of finding the cut-off radius for the construction of LDA-1/2 potentials by extrapolation. It was used to construct LDA-1/2 potentials for the semi-metal Bi in semiconductor compounds AlBi, GaBi and InBi, allowing for DFT calculations on dilute bismides with signifycantly reduced computational cost. In consequence, larger supercells, which are needed for low Bi concentrations, and dense k-point grids can be calculated. The usefulness of the approach for dilute bismides was demonstrated by calculating the electronic and optical properties of Ga(SbBi) for different Bi concentrations by using the results from the DFT calculations with the LDA-1/2 method as input to a microscopic theory.

References

[1] L. G. Ferreira, M. Marques, and L. K. Teles, AIP Advances **1**, 032119 (2011)

[2] V. Popescu and A. Zunger, Phys. Rev. B **85**, 085201 (2012)

[3] H. Haug and S. W. Koch, *Quantum Theory of the Optical and Electronic Properties of Semiconductors*, 5th ed. (World Scientific, Singapore, 2009)

[4] J. Hader, J. V. Moloney, and S. W. Koch, IEEE Journal of Quantum Electronics **41**, 1217 (2005)

Substrate, temperature and pressure effect (strain) on electronic properties of III-V semiconductor from ab-initio approach

Badal Mondal, Ralf Tonner

Institut für Physikalische und Theoretische Chemie, Universität Regensburg

Introduction

In the interest of deep and thorough understanding of pressure, temperature and substrate effect on the electronic properties (such as band structure) of ternary and binary III/V semiconductors we present here a systematic analysis of the above mentioned phenomena from modern *ab-initio* point of view using the more general strain model and the concept of theoretical epitaxy. In much more general footing we have modeled the above phenomena in terms of strain only; triaxial or isotropic, biaxial or in-plane strain, and uniaxial strain, for temperature, substrate, and perpendicular normal pressure effect respectively. Modeling this way gave us some additional advantages such as exploring in the (ultra-)high expansion limit in lattice constant, going beyond the experimentally achievable limit; expanding our realm of understanding by introducing the concept of isotropic compression and even doing (computational) experiment with hypothetical substrate, beyond the limits of only existed substrate. The use of perfectly flat substrate surface approximation in our model indirectly simplifies our total crystal lattice system by considering the lattice parameter of substrate as the only substrate property of interest in our problem and hence, avoiding consideration of any explicit substrate lattice during expensive density functional theory (DFT) calculation. Assuming the mutual independence and the thermal expansion of lattice constant as the major contributor, here we primarily focused on thermal expansion of lattice constant effect, separating from other temperature related phenomena (such as electron-phonon coupling etc.), as the effect of temperature on bandgap. Interestingly, due to the crystal symmetry, it turns out the case of perpendicular pressure application along (100) crystal direction in zincblende crystal (grown on (100) surface of another zincblende substrate), modeled by uni-axial strain can be treated in more general footing same as the case for bi-axial tensile strain. For current work, the well-known Ga(AsN) has been used for ternary model, and for binary model GaAs, GaP and some other well-known binary semiconductors are used. The bi-axial strain in analogy with real-world substrate constrain effect induced modification in the band structure shows an almost linear decrease in band gap in both tensile and compressive regions. A similar effect has also been observed under the investigation of isotropic strain effect. Going to the more simple binary cases we showed a direct-indirect transition in well-known direct bandgap semiconductor GaAs and vice versa for GaP. Under different strain conditions, we have found out semiconductor to metal as well as semiconductor to semi-metal transition in the semiconductor systems that we have considered here. Under biaxial tensile strain in GaAs, along with symmetry lowering mediated hh-lh splitting at Γ-point, we have discovered the shifting of hh-lh degeneracy point in k-space as well.

Results

For the analysis of Ga(AsN) we have used the same computational parameters from [1] with the needed additional modifications. For the layer grown on (100) substrate surface the variation of the bandgap with in-plane strain shows pretty good linear decrease under both tensile and compressive strain, irrespective of N-concentration, with a slop (or rate) of ~ 0.1 E_g/Strain (%) as is shown in Fig. 1a. A similar decreasing trend with varying slop depending on N-concentration has also been observed under isotropic tensile strain or thermal expansion (Fig. 1b). Comparing them together opens up a new way of multi-approach bandgap engineering strategy as is shown in Fig. 1c.

Analysis of the same on GaAs shows a direct to indirect bandgap transition at ~ 1.56 % of isotropic compressive strain and ~ 3.52 % of bi-axial tensile strain (within the limit of our computational resolution) (Fig. 2a). Going into more detail for isotropic compressive strain reveals 3 different transition points at ~ 1.56, 2.28, and 6.78 % of strain, associated with Γ to L, L to Δ_m (0, 0.43, 0.43) and Δ_m to X transition respectively (Fig. 2b). Examining the band structures in great detail we discovered the appearance of a completely new phenomenon, 'transient degeneracy'; at ~ 2.20 % of isotropic tensile strain in the CB at and near X-point, ~ 9.65 % isotropic compressive strain at and near Γ-point. Using very basic orbital analysis we found out the difference in orbital contributions at different symmetry k-points (Fig. 2c) is the primary reason for the transitions. This also showed the origin of 'transient degeneracy' being the 'exchange of orbital contributions'. Beyond ~ 6.67 % of isotropic tensile strain GaAs transit to 'zero bandgap' metalic state, which decreases to only ~ 2.85 % in GaSb.

For GaP we have shown an indirect to direct transition at ~ 2.63 % of isotropic tensile strain. Under bi-axial strain, the bandgap however remains indirect always, with the semiconductor to semi-metal transition at ~ 8.45 % of bi-axial tensile and ~ 9.83 % of bi-axial compressive strain (within the resolution limit of our calculations), Fig. 3.

Conclusion

In this project using *ab-initio* DFT calculation we showed that depending on the nature and the strength of applied strain in the system the material behaviour can change substantially, even the direct bandgap semiconductor can transform to indirect bandgap semiconductor or vice versa. Particularly we showed the transition of well-known direct bandgap semiconductor, GaAs to indirect bandgap, and well-known indirect bandgap semiconductor, GaP to direct bandgap. Combining the substrate and thermal effect we showed a multi-approach strategy for bandgap engineering in Ga(AsN). For GaAs, we have found out a completely new phenomenon, the appearance of 'transient degeneracy' and associated 'exchange of orbital contributions'. Nonetheless, other than certain experimental limitation in the present stage we believe that our this new analysis is quite significant, provides an extensive amount of hidden new insights even for otherwise extensively well studied materials, which hopefully lead and/or will find its way to the new application(s) (such as optical switch) in near future.

[1] Phil Rosenow et al., Phys. Rev. B 97, 075201 (2018).
[2] Ajit K. Katiyar et al., Sci. Adv. 6, eabb0576 (2020).

Outlook

To be more robust and unbiased one should consider using statistical sampling for the analysis of N-defect in Ga(AsN). Though through the symmetry forbidden band crossing argument we were able to explain the origin of 'transient degeneracy' and associated 'orbital exchange', however, the real consequences of these special states are still not clear to us and need to be further analyzed. Base on very primary intuition we believe that this special state would show special behaviour in electrical properties (such as electrical conductivity etc.) due to specialty in s- and p-character. Moreover, the alteration of s- and p-character along particular crystal direction in reciprocal space, near the critical strain regions would certainly have extreme significance yet to be discovered.

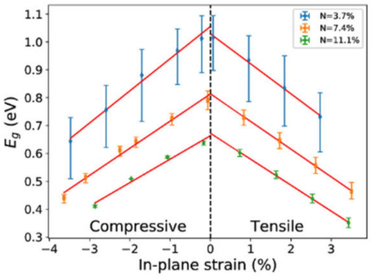

(1a)

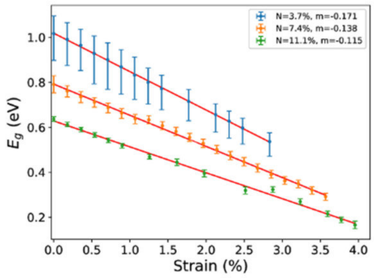

(1b)

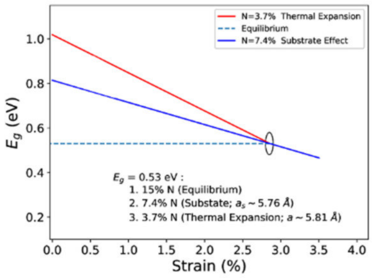

(1c)

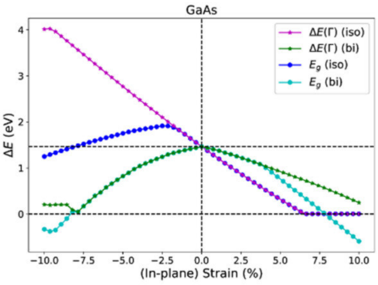

(2a)

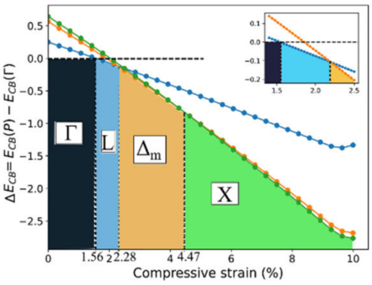

(2b)

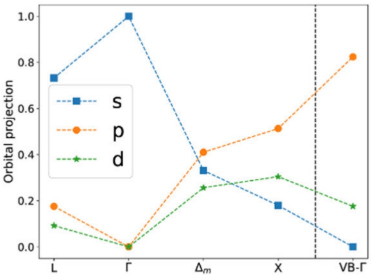

(2c)

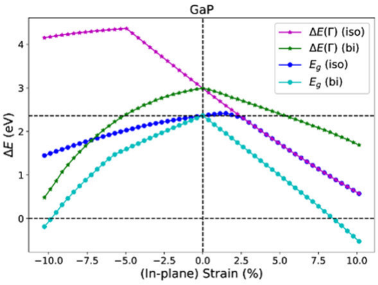

(3)

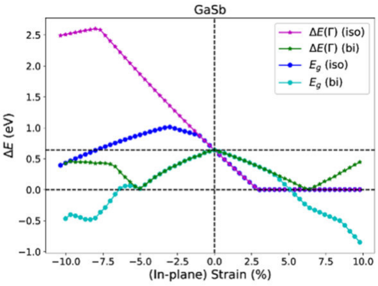

(4a)

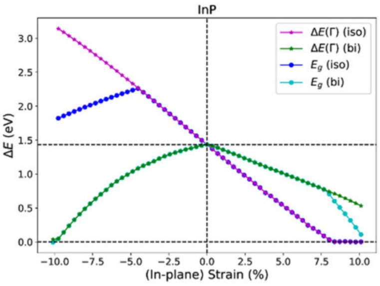

(4b)

Automated exploration of reaction networks in chemical vapor deposition by density functional theory

Fabian Pieck[1], Ralf Tonner[1]

[1]*Institute of Physical and Theoretical Chemistry, Universität Regensburg*

The gas phase decomposition of triethylgallane[1], tert-butylphosphine (TBP)[1], trimethyl- and triethylboron[2] and di-tertiary-butyl-arsano-amine[3] already results in reaction networks spanning more than 60 elementary reactions. However, a proper model for the whole CVD process (Fig. 1) must include the substrate surface. The interactions between precursor and surface alter the decomposition channels, while additional novel reactions appear.

The calculation of all elemental reactions by periodic density functional theory is a demanding task. Therefore, we are developing a systematic and automated procedure to explore the surface reaction network. In this way we can reduce the manual effort and the possibility to miss an important reaction channel. Furthermore, by implementing an efficient Message Passing Interface (MPI) parallelization we can exploit modern high-performance computers.

Our approach consists of three main steps: In a first step, the adsorption minima for the precursor of interest are calculated. This is achieved in a brute force manner by running a set of structural optimizations in which the molecule is systematically placed above the surface. Linking every observed structure to its final adsorption minimum enables to derive the so-called adsorption basin. We attribute this basin to a probability distribution for the adsorption in a certain minimum. In a second step all decomposition products are created. Here, we use a distance criterium to identify bonded atoms in the precursor. By breaking and rearranging bonds, all decomposition products are formed. In a third step, reaction paths connecting individual structures are automatically selected and calculated. The reaction path optimization is done by a tailored and improved implementation of the nudged elastic band (NEB) method. Furthermore, internal coordinates are exploited for the initial path interpolation.

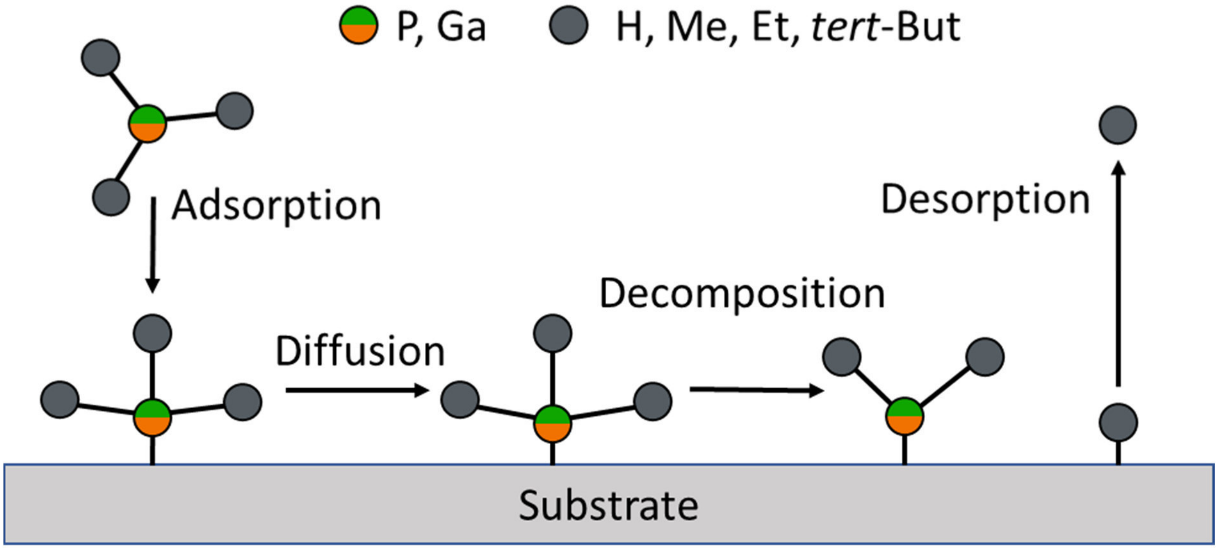

Fig. 1: Schematic overview of the elemental steps in the chemical vapor deposition. The surface reaction network consists of energetic minima (structures) and reaction paths connecting the minima (arrows).

Recent test runs for Bi, GaH_3 and TBP on GaP(001) have partly suffered from instabilities in the NEB algorithm. These instabilities must be addressed by either fine tuning the parameters controlling the algorithm or by improving the algorithm itself. Furthermore, safety checks are necessary to detect and interrupt problematic reaction path calculations as soon as possible. Unfortunately, some manual interventions would then be inevitable. Another finding emerged in the test runs is that the used computing time is considerably rising with larger molecules like TBP. One major reason is the increased number of degrees of freedom for larger molecules, which leads to more iterations in every optimization algorithm. To reduce the computing time, we are planning to utilize a gaussian process regression (GPR) approach, which is one of the heavily used machine learning algorithms. The advantage of a GPR approach is, that it can be merged with DFT calculations.[4] Switching between forces derived by DFT and GPR calculations enables us to speed up our calculations, while maintaining the accuracy at the DFT level of theory.

References

[1] A. Stegmüller, P. Rosenow, R. Tonner, *Phys. Chem. Chem. Phys.* **2014**, *16*, 17018.

[2] a) M. Imam, K. Gaul, A. Stegmüller, C. Höglund, J. Jensen, L. Hultman, J. Birch, R. Tonner, H. Pedersen, *J. Mater. Chem. C* **2015**, *3*, 10898; b) M. Imam, L. Souqui, J. Herritsch, A. Stegmüller, C. Höglund, S. Schmidt, R. Hall-Wilton, H. Högberg, J. Birch, R. Tonner, H. Pedersen, *J. Phys. Chem. C* **2017**, *121*, 26465.

[3] E. Sterzer, A. Beyer, L. Duschek, L. Nattermann, B. Ringler, B. Leube, A. Stegmüller, R. Tonner, C. von Hänisch, W. Stolz, K. Volz, *J. Cryst. Growth* **2016**, *439*, 19.

[4] O.-P. Koistinen, F. B. Dagbjartsdóttir, V. Ásgeirsson, A. Vehtari, H. Jónsson, *J. Chem. Phys.* **2017**, *147*, 152720.

The influence of growth interruption on the luminescence properties of Ga(As,Sb)-based type II heterostructures

Luise Rost, Jannik Lehr, Milan Maradiya, Lukas Hellweg,
Wolfgang Stolz and Wolfram Heimbrodt

Department of Physics and Material Sciences Center, Philipps-Universität Marburg

Introduction

Infra-red semiconductor lasers for long-range optical communication using optical fibers are still a highly topical field. There are many ways to achieve long wavelength lasing in the range of 1.3 µm.

A strategy to get to longer wavelength and to overcome Auger losses is the use of type-II devices, where the recombining electrons and holes are spatially separated[1,2]. Additionally, such systems offer more degrees of freedom for device design as the band edges of the electron and the hole confining wells can be varied independently allowing for a wide tuning of the type-II transition energy. A promising heterostructure design for such applications are so called W-laser structures, which enable the optimization of the wave function overlap by adding barrier layers to confine carriers. With the continuing progress of device miniaturization in mind, the properties of the internal interfaces are getting more and more important. In this study, we present as thorough investigation of photoluminescence properties of (Ga,In)As/GaAs/Ga(As,Sb) heterostructures with modified interface morphology.

Results

In a previous paper we could show that one can improve the type II photoluminescence efficiency by smoothening the interface of (Ga,In)As[3]. As extremely sensitive probe the type II recombination has been used of (Ga,In)As/GaAs/Ga(As,Sb) double quantum well (DQW) heterostructures. By applying a 120s growth interruption (GI) after growth of the (Ga,In)As layer and prior to the growth of the next layer a smoothening of the interface and enhanced luminescence efficiency was found. A detailed analysis of the other relevant layer Ga(As,Sb) and its relevance for a high quantum efficiency of the W-laser is missing so far.

We used the inverted DQW Ga(As,Sb)/GaAs/(Ga,In)As to analyze the influence of GI on the morphology of Ga(As,Sb) layers and the luminescence properties, particularly the recombination dynamics of the charge transfer (CT) recombination processes. We were able to reveal the strong correlation of the type II luminescence intensity and lifetime with the morphology of the Ga(As,Sb) layer and interfaces.

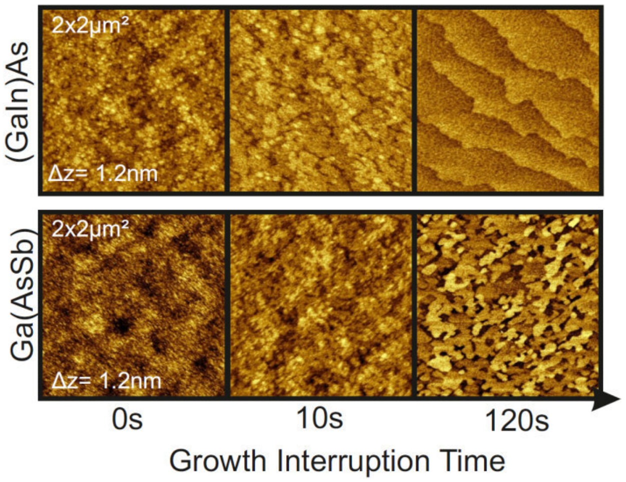

Fig. 1: Atomic Force Microscopy Images after selective etching to the interior interface of the respective layer

We were able to reveal a correlation of the morphology of Ga(As,Sb) interfaces and charge transfer PL intensity and lifetime. GI with only TBAs stabilization results in a substantial Sb loss, as was observed by combining HR-XRD and AFM analysis, yielding a rough Ga(As,Sb) interface, deep holes and even an effectively reduced Ga(As,Sb) layer thickness. This results in a substantially reduced type II PL intensity and recombination time at room temperature with increasing GI time. The morphology changes due to the Sb loss cause an increasing number of non-radiative centers.

It was found, that this deterioration of the interface could be overcome with Sb precursor TESb present during the GI additionally. This suppresses the sublimation loss of Sb atoms and results in smooth interface with strongly reduced number of non-radiative centers. The cw-PL intensity is substantially enhanced using 10s GI. Even the type II recombination time is enhanced due to the suppressed loss channel. The achieved high quality of the Ga(As,Sb)/GaAs interface could be convincingly shown by the temperature dependent PL measurements. The Type II recombination of the non-localized carriers and excitons could be observed down to lowest temperatures. The localized carriers could be hardly seen, since the number of hole trap states is obviously substantially reduced. It is important to note, however, that there is an optimal GI-time. A too long GI leads again to a degradation of the interface.

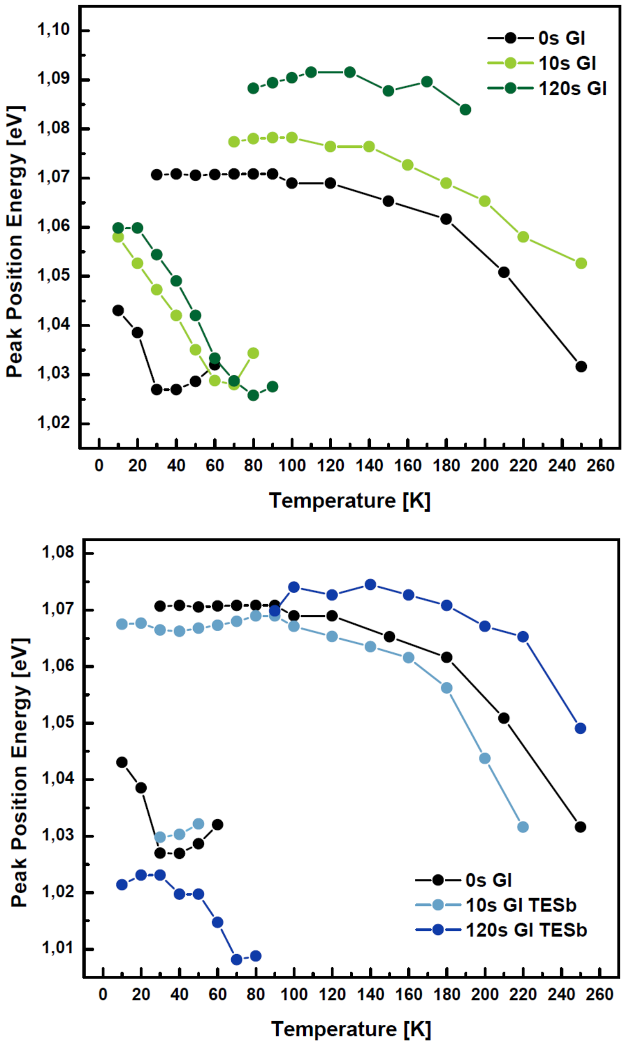

Fig. 2: Peak Position Energy over temperature. The connections between the different temperatures are only a guide to the eye. a) Depicted in green are the samples with 10s and 120s GI and b) the samples with additionally TESb during 10s and 120s GI.

Outlook: what is planned?

We like to further investigate the recombination dynamics of charge transfer processes at 10 K, to establish a kinetic model. Furthermore we want to analyze the temperature depended behavior of the band off set of the type II transition.

References

[1] C. Berger, C. Möller, P. Hens, C. Fuchs, W. Stolz, S. W. Koch, A. Ruiz Perez, J. Hader, and J. V. Moloney, AIP Adv. **5**, 047105 (2015).

[2] S. Gies, C. Kruska, C. Berger, P. Hens, C. Fuchs, A. Ruiz Perez, N. W. Rosemann, J. Veletas, S. Chatterjee, W. Stolz, S. W. Koch, J. Hader, J. V. Moloney, and W. Heimbrodt, Appl. Phys. Lett. **107**, 182104 (2015).

[3] L. Rost, S. Gies, M. Stein, C. Fuchs, S. Nau, P. Kükelhan, K. Volz, W. Stolz, M. Koch, and W. Heimbrodt, J. Phys. Condens. Matter **31**, (2019).

Optoelectronic Coupling between Colloidal Quantum Dots and semiconductor substrates

Mikko Wilhelm and Wolfram Heimbrodt

Department of Physics and Material Sciences Center, Philipps-Universität Marburg

Introduction

The optoelectronic interaction between colloidal II-VI semiconductor quantum dots (QDs) and different semiconductor substrates is studied. The colloidal quantum dots provide a simple and low-cost way to functionalize the semiconductor substrates with a variety of physical properties by modifying the size, shape, and composition of the quantum dots. Such hybrids are promising systems for applications as gas sensors, photo sensors or solar cells.

In this work CdS/ZnS and CdSe/ZnS core shell quantum dots are transferred from solution via knife coating to the substrates to create a thin layer of quantum dots linked via Van der Waals interaction to the substrate. Different substrates like ZnSe, ZnMnSe, GaP, TiO_2 and quartz are used. The aim is to investigate and describe the interaction between the QDs and semiconductor substrates, especially regarding energy and charge transfer in these hybrid structures.

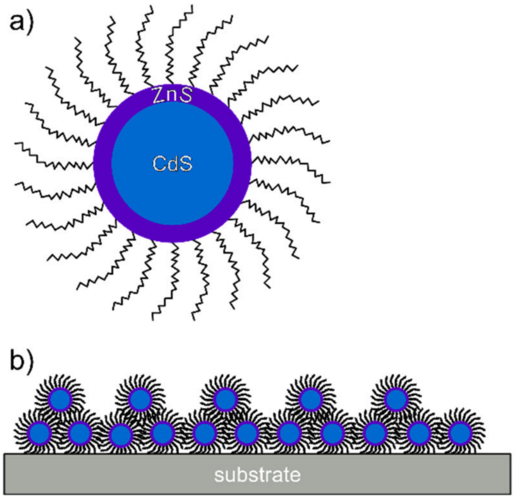

Fig. 1: Schematic representation of the quantum dots and aa dried layer on the semiconductor substrate.

Results

The hybrid structures were characterized by continuous-wave and nanosecond time-resolved photoluminescence measurements at different temperatures. The dominant transfer processes between the QDs and the substrate depend on the distance and the band alignment in the coupled structures. It is well known that the band gap E^{QD} of the QDs is dependent on their radius R and the effective masses of the electron and hole m^* according to the Brus equation:

$$E^{QD} = E_{gap} + \frac{h^2}{8\,R^2}\left(\frac{1}{m_e^*} + \frac{1}{m_h^*}\right) - \frac{1.8\,e^2}{4\,\pi\,\varepsilon_0 \varepsilon_r R}$$

Thus, it is possible to tune the band alignment and with it the transfer processes in the hybrid structures by using quantum dots of different sizes. The effect of the size on the PL spectra and band alignment for the quantum dots on a ZnSe substrate is shown in Fig. 2. Energy transfer from the quantum dots should be possible if their band gap is larger than the band gap of the substrate. Electron transfer can happen from the higher energy band to the lower band. In all cases, only the quantum dots close to the interface participate in the transfer processes. That is why it is important to create thin layers of quantum dots. Absorption measurements of prepared quantum dots on quartz indicate a layer thickness of only very few monolayers. The transfer process can be investigated with the decay curves of the respective photo-luminescence bands, as shown in Fig. 3. Quantum dots on quartz are taken as a reference. The PL is observable for hundreds of nanoseconds after excitation. Additional transfer processes lead to a faster PL decay.

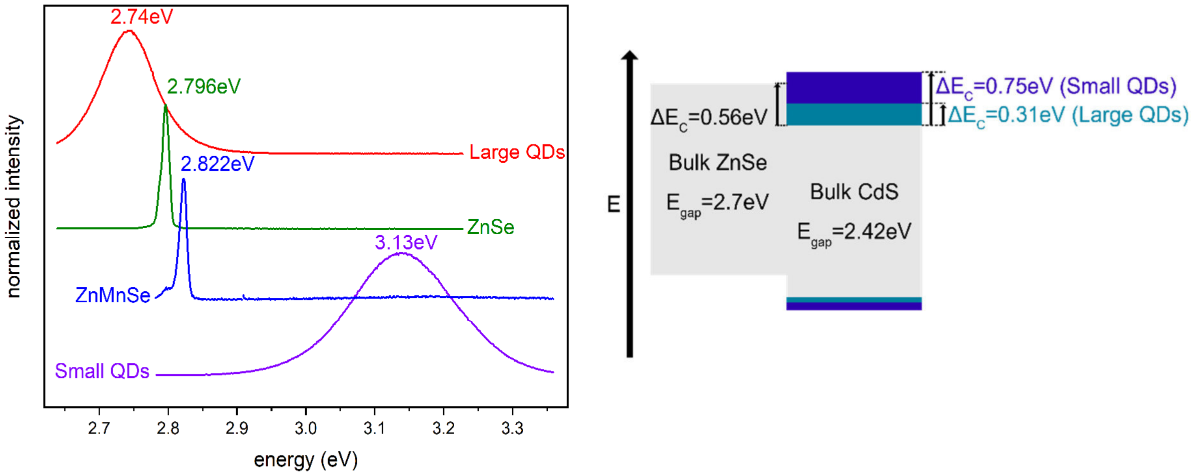

Fig. 2: Left: PL spectra at T=10K for small and large quantum dots and the ZnSe substrates
Right: Estimated band alignment between the quantum dots and the substrate at T=290K.

To quantitatively describe the PL decay the curves can be fitted with the following equation, assuming a distribution of decay times $\rho(\tau')$, an average transfer time τ_{trf} and triplet feeding time τ_{trip}:

$$I(t) = \left(1 - c + c\exp\left(\frac{-t}{\tau_{trf}}\right)\right) A_0 \int_0^\infty \rho(\tau')\exp\left(\frac{-t}{\tau'}\right) d\tau' + (1-c)\,B_0\,\exp\left(\frac{-t}{\tau_{trip}}\right)$$

The kind of transfer processes is then determined comparing different hybrid structures with different band alignments. A strong transfer can be observed for high energy quantum dots on ZnSe, this transfer is impaired when the ZnSe is doped with manganese or when lower energy quantum dots are used.

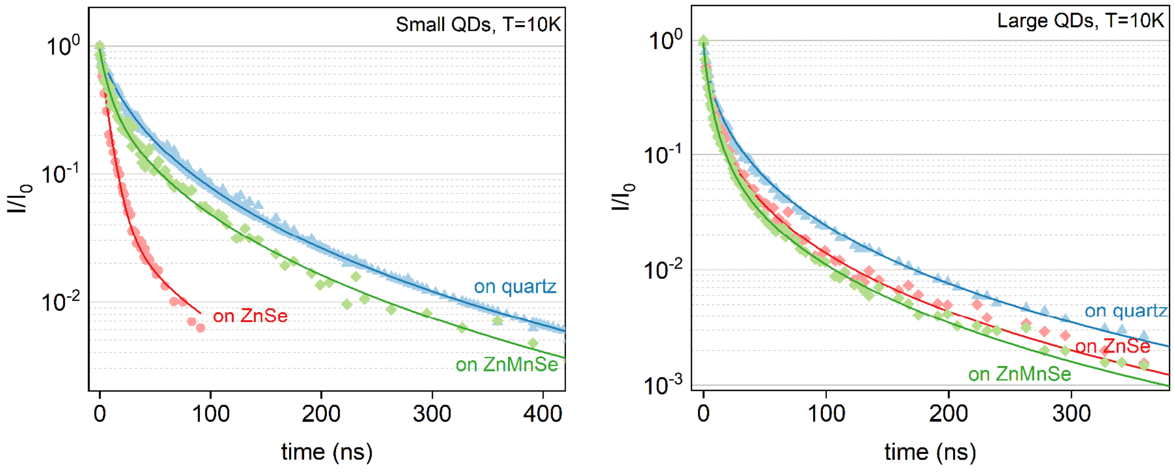

Fig. 3: Photoluminescence decay curves of the small QDs (left) and large QDs (right) on different substrates. The curves are fitted according to equation (2).

Conclusion

The energy and charge transfer processes in hybrid structures consisting of core shell CDs and semiconductor substrates was studied. It was possible to prepare these hybrid structures with a thin layer of quantum dots by using a simple and low-cost method. A transfer from the quantum dots to suitable substrate could be observed. The transfer mechanism is changed by using quantum dots of different sizes. If possible, an electron transfer process is more dominant than an energy transfer.

Analyzing the influence of different growth parameters on the decomposition of MOVPE precursors with mass spectrometry

J. Haust, O. Maßmeyer, W. Stolz and K. Volz

Department of Physics and Material Sciences Center, Philipps-Universität Marburg

Introduction

While Metal-organic vapor phase epitaxy is widely used to produce all kinds of electronic devices like Lasers, LEDs, transistors and many more[1], the actual growth process in the reactor is still not fully understood.

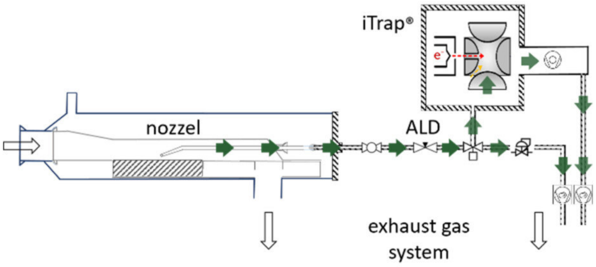

Fig. 1: Experimental setup[2].

To address this issue insitu investigation of the MOVPE process are a possibility. With the quadrupole ion trap mass spectrometer, which was used for this work, integrated in the MOVPE system the analysis of the gas phase composition is possible[2]. This allows to investigate the influence of the growth parameters like the reactor pressure, the total flow rate in the reactor or the source flow on the decomposition of the metalorganic precursors *tert*-butylarsine (TBAs) and *tert*-butylphosphine (TBP). A nozzle, as shown in Fig. 1, collects a small amount of gas in the reactor, pulses it through an atomic layer deposition valve (ALD) in the ion trap and the fast Fourier transformation based concept allows the recording of a whole mass spectrum in less than two seconds[3]. This and the possibility of very sensitive ionization parameters combined with the high sensitivity of the spectrometer makes this setup to a powerful tool for the analyzation of small amounts of large organic molecules, which are typically used in a MOVPE process.

Result and Conclusions

Fig. 2 shows the unimolecular decomposition curves for TBAs with different reactor pressures. The experimental data in the temperature range from 300 °C to 800 °C is fitted with a sigmoidal step function. The decomposition temperature T_d is determined as the temperature at which the intensity of the curve goes down to half of the initial value. The determined decomposition temperature shows a decreasing linear trend with increasing reactor pressure. This is an expected behavior, because the temperature in the experiment is measured in the suszeptor, the gas is collected a few centimeter above it and the thermal conductivity of a gas increases with higher density[4]. For TBAs there were also similar decomposition curves obtained while changing the total or the source flow rate while keeping the other parameters constant. While the total flow rate seems to have no influence on the determined decomposition temperature, it increases with a higher source flow. However in the literature the decomposition temperature of TBAs shows no dependence of the partial pressure[5].

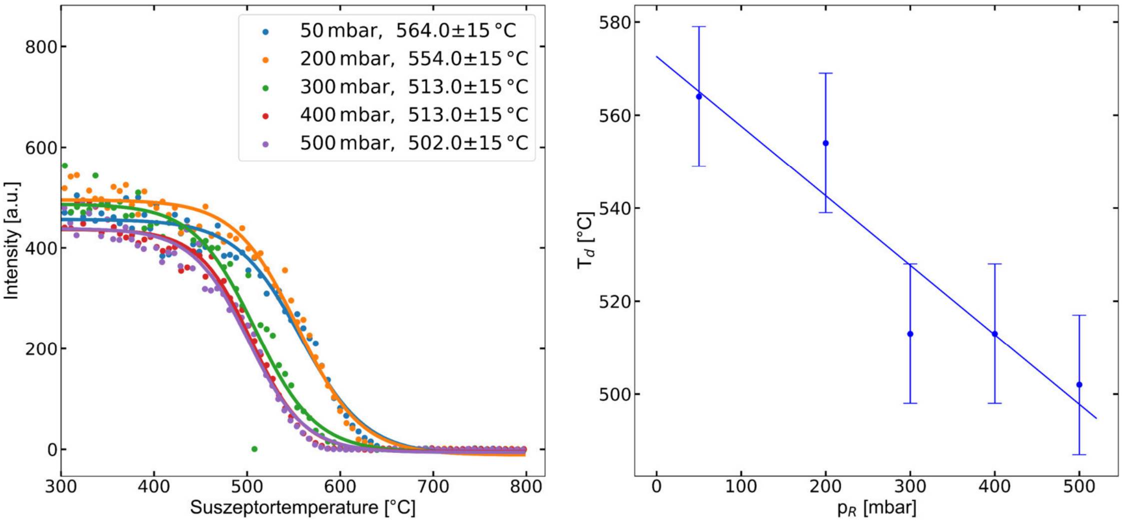

Fig. 2: Decomposition curves for TBAs (mass 134 amu) with a total flow rate of 6800 sccm, a source flow of 11 ml and different reactor pressures p_R (left) and the evaluated decomposition temperature T_d for the respective reactor pressures (right).

While investigating TBP the nozzle, which collects the gas in the reactor, was unwillingly covered with phosphor. Before the nozzle was covered the determined decomposition temperature is 654 °C at a total flow rate of 6800 sccm, a source flow of 5.8 ml/min and a reactor pressure of 50 mbar. With a covered nozzle the determined decomposition temperature is 715 °C under the same growth parameters, which leads to the conclusion, that the surface plays an important role for the decomposition.

Detailed information and interpretation of the results including experiments with N_2 as carrier gas instead of H_2 will be discussed in the presentation.

Outlook

So far only two group V precursors were investigated. There exist several more precursors also for the group III compounds like trimethylgallium (TMGa) or trimethylalluminium (TMAl), which can be investigated. The next step is to examine how the growth parameters, like reactor pressure or total flow rate, have an influence on the bimolecular reactions of two different precursors in the reactor.

References

[1] G. B. Stringfellow, “Fundamental Aspects of MOVPE,” in Metalorganic Vapor Phase Epitaxy (MOVPE), Wiley, 2019, pp. 19–69.
[2] L. Nattermann et al., “An experimental approach for real time mass spectrometric CVD gas phase investigations,” Sci. Rep., 2018, vol. 8, no. 1, pp. 1–7.
[3] H. Y. Chung et al., “Very sensitive real-time inline process mass spectrometer based on FFT Ion Trap technique,” 2016, 27th Annual SEMI Advanced Semiconductor Manufacturing Conference (ASMC), pp. 263–266.
[4] W. Demtröder, Experimentalphysik 1, Springer Berlin Heidelberg, 2015.
[5] C. A. Larsen, N. I. Buchan, S. H. Li, and G. B. Stringfellow, “Decomposition mechanisms of tertiarybutylarsine,” J. Cryst. Growth, 1989, vol. 94, no. 3, pp. 663–672.

Bismuth containing W type laser structures for long wavelength emission on GaAs substrates

T. Hepp[1], J. Veletas[2], R. Günkel[1], O. Maßmeyer[1], J. Glowatzki[1], S. Chatterjee[2] and K. Volz[1]

[1]Department of Physics and Material Sciences Center, Philipps-Universität Marburg
[2]Institute of Experimental Physics I, Justus-Liebig-Universität Gießen

In this work we will present the growth of Ga(N,As)/Ga(As,Bi)/Ga(N,As) W type structures (WQW) grown on ex. GaAs (001) in terms of the challenges occuring during growth. Further, we will discuss our first results on laser test structures utilizing WQWs as active region. These WQWs can be grown strain balanced on GaAs, since Ga(As,Bi) is compressively strained while Ga(N,As) is tensile strained. Due to the strong reduction of the band gap by incorporation of nitrogen (N) and bismuth (Bi) respectively, it is possible to shift the emission wavelength of such structures into the mid infrared region for application as telecom lasers[1].

The samples were grown in an AIXTRON AIX 200 horizontal reactor system. Triethylgallium (TEGa), tertiarybutylarsane (TBAs), 1,1-dimethylhydrazine (UDMHy) and trimethylbismuth (TMBi) were chosen as precursors. The layer thicknesses and compositions were determined using high resolution X-Ray diffraction (HR-XRD). A frequency doubled Nd:YAG laser was used for excitation of the samples to record the photoluminescence (PL) signal. The sample surface was investigated using an atomic force microscope (AFM).

Fig. 1 a) shows an HR-XRD diffractogram of a Ga(N,As)/Ga(As,Bi)/Ga(N,As) WQW. The clear appearance of pendellösung fringes coupled with good agreement between dynamic modelling and experimental data suggests abrupt interfaces between the different material systems. Moreover, the desired thickness and incorporation of the respective QWs was achieved.

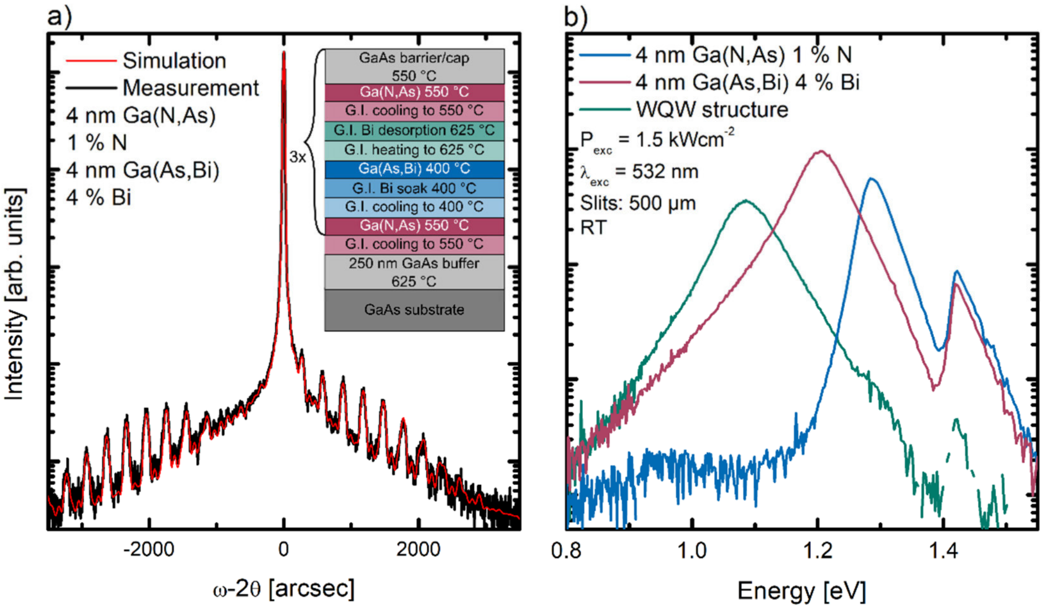

Fig. 1: a) Shows an HR-XRD diffractogram of a Ga(N,As)/Ga(As,Bi)/Ga(N,As) WQW and corresponding modeling. The inset sketches the grown sample structure. A good fit between the modeled and experimental diffractogram suggest abrupt interfaces. b) Shows the PL spectra of the WQW (green) as well as the respective Ga(N,As) (blue) and Ga(As,Bi) (red) test structures. The PL of the WQW is clearly red shifted compared to the type I test structures, proving the type II transition in the WQW.

The inset shows the rather complex growth sequence of the sample. The necessity of the different steps will be discussed in the presentation.

The corresponding PL spectrum of this sample is shown in Fig. 1 b) together with the PL spectra of test structures, consisting of three Ga(N,As) and Ga(As,Bi) QWs, respectively. A clear red shift of the PL peak from the WQW compared to the PL peak of both test structures is observed, proving the domination of the type II transition in the WQW. The PL peak around 1.1 eV is a good starting point for experiments to shift the emission wavelength further into the infrared. Shifting the emission wavelength will be achieved by increasing the N fraction of the Ga(N,As) QWs.

The PL of three WQWs consisting of a Ga(As,Bi) QW with 4 % Bi incorporation is shown in Fig. 2, with increasing N fraction of the Ga(N,As) QWs from 1 % up to 5.0 % N to shift the emission to longer wavelengths. For WQWs with higher N fractions the emission wavelength approaches the wavelengths suitable for telecommunication applications.

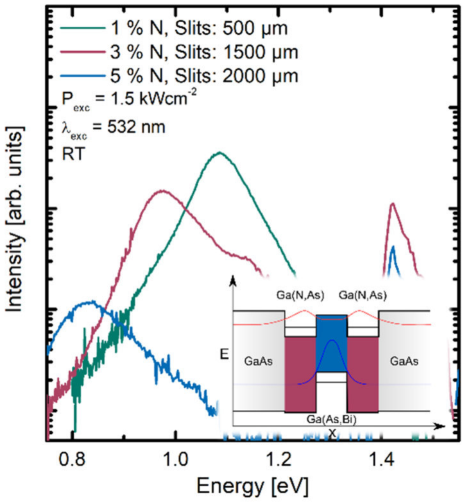

Fig. 2: PL spectra of three WQWs with increasing N fraction in the Ga(N,As) QWs. The Bi fraction was kept constant at 4 % Bi for all experiments. The increased N fraction leads to a clear red shift of the PL peak position. Sketch of the resulting band structure of a WQW as inset.

Though very promising, the combination of these highly mismatched alloys poses severe growth challenges. The deposition of Ga(As,Bi) requires low growth temperatures around 400 °C and growth interruptions are needed in order to apply temperature changes after deposition of the QWs since Ga(N,As) and GaAs are grown at 550 °C (compare inset of Fig. 1 a)). Moreover, Bi tends to segregate to the surface, which reduces the incorporation of N[2]. These challenges and suitable solutions will be discussed in detail during the presentation.

Furthermore, based on these WQWs laser test structures were fabricated. The corresponding laser characteristics will be presented and discussed with respect to the growth challenges mentioned before.

To understand the problems arising at the Ga(N,As)/Ga(As,Bi) interface, RAS experiments will be carried out to investigate the surface reconstruction during the Bi soak. The finding will be used to change the growth sequence in order to realize symmetric WQW structures. Furthermore, the integration of very thin GaAs barriers sandwiched in the Ga(N,As)/Ga(As,Bi) and Ga(As,Bi)/Ga(N,As) interface will be investigated.

References

[1] C. A. Broderick et al., Sci. Rep. 7, 46371 (2017)
[2] F. Dimroth et al., J. Appl. Phys. 91, 3687 (2002)

In-situ analysis of Ga(N,As)/Ga(As,Bi) interfaces during growth by MOVPE

R. Günkel, T. Hepp, O. Maßmeyer and K. Volz

Department of Physics and Material Sciences Center, Philipps-Universität Marburg

Various optoelectronic devices are based on a mid-infrared optical transition, like solar cells, photodetectors and light emitters. A promising candidate for such devices are Ga(N,As)/Ga(As,Bi) heterojunctions, which have type II band alignment tunable by incorporation of the dilutes N and Bi, respectively. Even Ga(N,As)/Ga(As,Bi)/Ga(N,As) so called W-type structures on GaAs (001) substrates may provide a near infrared telecom lasers[1-2].

The MOVPE growth of these samples is quite challenging. Firstly, the deposition of the Ga(As,Bi) QWs is conducted at 400 °C to achieve a significant Bi incorporation. Secondly, the Ga(N,As) QWs are grown at 550 °C to reduce the incorporated defects usually present during low T growth. Therefore, several temperature steps are need for one sample. The current challenge is to get well-defined interface without grading layers or an increase of roughness of the present interrfaces interfaces. The precursors used are triethylgallium (TEGa) for Ga supply, tertiarybutylasane (TBAs) for As supply, 1,1-dimethylhydrazine (UDMHy) for N supply, trimethylbismuth (TMBi) for Bi supply and tributylphosphine (TBP) for P supply. To enable a smooth Ga(As,Bi) layer growth, it is necessary to cover the surface of the substrate with Bi before the actual growth of Ga(As,Bi) by a preflux of TMBi[3]. The cooling of the reactor system takes seven minutes between 550 °C used for Ga(NAs) growth and 400 °C necessary for Bi preflux and growth. During the cooling phase, different precursors were offered to stabilize the surface, for example TBAs or TBAs and UDMHy. After the cooling down, the usual TMBi preflux is supplied. High resolution X-ray diffraction (HR-XRD) was used to determine the layer thickness and composition. The goal of the present work was to investigate the Ga(N,As)/Ga(As,Bi) interface, which showed some issues in previous experiments.

To investigate the interface quality during several growth experiments, it was chosen to use reflectance anisotropy (RA) measurements as main method to get a non-destructive and direct feedback. In this type of spectroscopy, the incoming, quasi perpendicular linear polarized light is reflected and the difference of reflectivity of both surface directions (-1,1,0) and (1,1,0) is normalized by the total reflectivity. Furthermore, the RA spectra are correlated to surface reconstruction, which in turn depend on the composition and strain of fewer upper atomic layers. Those spectra can be used as fingerprints to compare or identify different surface reconstructions. In contrast, the quantitative interpretation of such measurements is elaborate and requires further research. By in-situ analyzing through the RA spectra, it is possible to determine the current surface reconstruction by comparing to measurements with known surfaces[4]. Due to the low temporal resolution of our setup, repeated measurements could only be made during the growth of quantum films at one fixed energy. In the following, this kind of measuring is called RA transient.

In Fig. 1a) there are shown different RA spectra of different layers, which will be used in targeted type II structure. The difference between Ga(As,Bi) growth (pink curve) and Ga(As,Bi) stabilized under TBAs supply (red curve) is induced by the TEGa supply during growth. To investigate growth of the type II structure in-situ, based on the differences in the RA spectra in 1a), the energy 1.52 eV was chosen for further transient measurements. As outcome to the experiments, which are plotted in Fig. 1 b), the time of the TMBi preflux was shortened from

90 s to 30 s due to more or less stable signal after 30 s up to 40 s without any stabilizing precursors (black curve). Moreover, there is no noticeable difference between a TBAs (yellow curve) and simultaneously TBAs and UDMHy (green curve) stabilization.

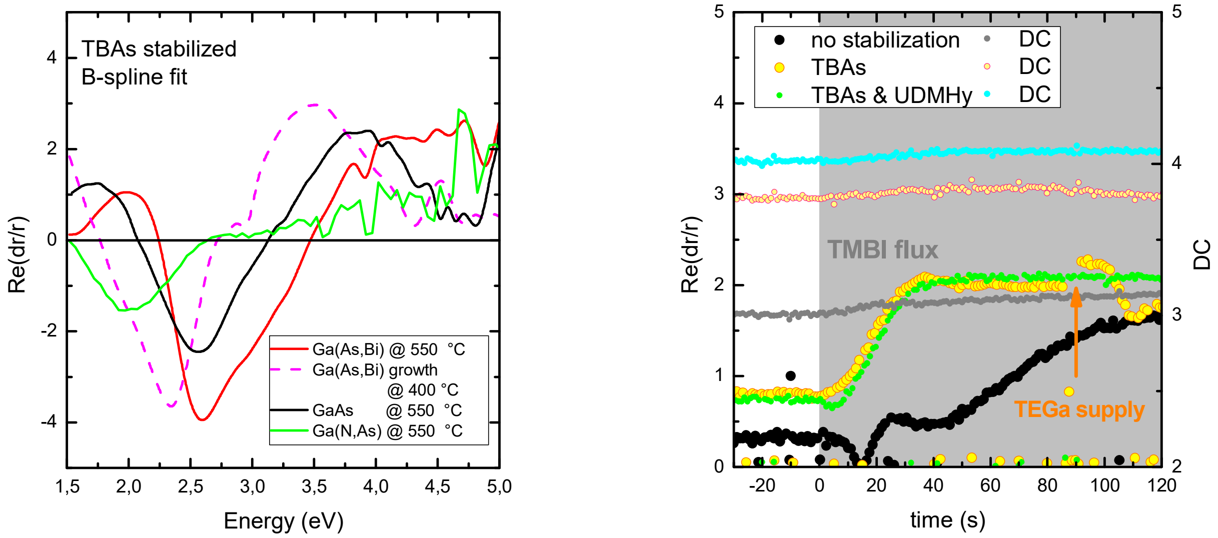

Fig. 1: a) RA spectra at 550°C with TBAs stabilization of Ga(N,As) (green), Ga(As,B)i (red) and GaAs (black);the spectra of Ga(As,Bi) is changed from red to pink by TEGa supply. b) RA transient and DC voltage at fix energy of 1,52 eV during growth: At 0 s the TMBi is supplied as preflux (grey background). At 90 s the TEGa is supplied (only yellow curve). There is no significant decrease in DC observed during TMBi preflux with or without any stabilization treatment. Since the DC value depends directly on the reflected intensity, which in turn is determined by the surface roughness and the material composition, it could be estimated that no significant increase of roughness takes place.

Outlook

In order to proof our current results and interpretation, TEM measurements will be carried out in future.

For further investigations on the influence of Bi deposition on tensile strained layers like Ga(N,As) oder Ga(P,As), the Bi pre-treatment could be attached to Ga(N,As) and Ga(P,As) bulk structures without a GaAs cap. After growth by MOVPE, the deposed Bi will be selectively etched by sulfuric acid[5] and not used to enable Ga(As,Bi) growth. The samples surface roughness, thickness and composition will be analyzed by atomic forced microscopy (AFM) and HR-XRD before and after etching and in comparison, to samples without any Bi treatment.

References

[1] J. Hwang, J. D. Phillips, (2011). Band structure of strain-balanced GaAsBi/GaAsN superlattices on GaAs. *Physical Review B, 83* (19), 195327.

[2] C. A. Broderick, S. Jin, I. P. Marko, K. Hild, P. Ludewig, Z. L. Bushell, W. Stolz, J. M. Rorison, E. P. O'Reilly, K. Volz, and S. J. Sweeney, (2017). GaAs$_{1-x}$Bi$_x$/GaN$_y$As$_{1-y}$ type-II quantum wells: novel strain-balanced heterostructures for GaAs-based near-and mid-infrared photonics. *Scientific reports,* 7, 46371.

[3] O. Maßmeyer, T. Hepp, R. Günkel, J. Glowatzki, W. Stolz, and K. Volz, (2020). In situ Analysis of Bi terminated GaAs (001) and Ga (As, Bi) Surfaces during Growth by MOVPE. *Applied Surface Science*, 147401.

[4] P. Weightman, D. S. Martin, R. J. Cole, and T- Farrell, (2005). Reflection anisotropy spectroscopy. *Reports on Progress in Physics, 68* (6), 1251.

[5] E. Sterzer, N. Knaub, P. Ludewig, R. Straubinger, A. Beyer, and K. Volz, (2014). Investigation of the microstructure of metallic droplets on Ga(AsBi)/GaAs. *Journal of crystal growth, 408*, 71-77.

Further research summaries by GRK-members

(in alphabetical order)

Investigation of the ultrafast dynamics of electronic and vibronic excitations at the GaP/Si-interface

Tim Bergmeier

Department of Physics and Material Sciences Center, Philipps-Universität Marburg

The charge dynamics at buried semiconductor interfaces are an important factor determining the performance of any built device, whose function is relying on semiconductor heterostructures. To investigate those dynamics, a noninvasive, highly interface sensitive technique is the measurement of the second harmonic (SHG) of an incoming probe-beam generated within the sample, with the latter consisting of a GaP/Si(001)-heterostructure serving as a model system for a heterostructure of a polar and a nonpolar material. By using a pump-probe scheme, pump-induced changes in the probe-induced SHG can be measured time-resolved by varying the distance between pump- and probe-pulse.

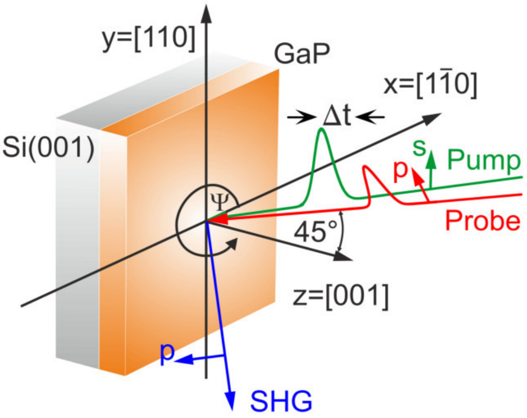

Fig. 1: Schematic view of the experimental setup used for SHG-measurements. The pump (green) induces a change in the SHG (blue) generated by the probe (red)[1].

I want to further characterize the newly found interface-specific low-frequency phonon mode of GaP/Si(001), which was first measured by using coherent phonon spectroscopy and has a frequency of 2 THz[2], through energy- and fluence-dependent SHG-measurements. Furthermore, I would like to search for other interface-specific phonon modes, such as a longitudinal-optical (LO) mode with higher frequency. Also, I would like to do similar SHG-measurements on other suitable material systems such as GaP/Si(112) or GaAs/Ge. Especially the results of the measurements on GaP/Si(112) compared to the ones on GaP/Si(001) could be very interesting, since the (001)-interface tends to a pyramidal structuring due to the polarity of the interface[3]. This effect could be weakened by growing on substrates oriented in the (112)-direction, which would then lead to the interface being a more abrupt. This should affect the results in showing more distinct resonant modes.

References

[1] G. Mette et al., Femtosecond time-resolved nonlinear optical spectroscopy of charge transfer at the buried GaP/Si(001) interface, under review, 2020

[2] K. Ishioka et al., Sub-picosecond acoustic pulses at buried GaP/Si interfaces, Appl. Phys. Lett. **111**, 062105 (2017)

[3] A. Beyer et al., Pyramidal structure formation at the interface between III/V semiconductors and silicon, Chem. Mater. **28**, 3265-3275 (2016)

Energy-filtered STEM – an experimental study using a fast, pixelated detector

S. Firoozabadi, A. Beyer, P. Kükelhan, K. Volz

Department of Physics and Material Sciences Center, Philipps-Universität Marburg

Introduction

Taking into account only elastic scattering, quantitative agreement between high angle annular dark field STEM (HAADF- STEM) images and complementary multi-slice image simulations at atomic scale was achieved[1]. However, the demand of STEM measurements at low angles was increased recently by the advent of four dimensional STEM using the ultra-fast pixelated camera. Applications include light element detection and dislocation characterization by enhanced annular bright-field imaging or electric field measurement by center of mass (COM)[2]. Nonetheless, it was proved that there is a discrepancy between image simulations and experiments at low-angles, which could be caused by neglecting the inelastic scattering in the image simulations[3]. In this study, the experimental convergent beam electron diffraction (CBED) images taken by a fast, pixelated detector is compared to the simulated CBED images in which the plasmon scattering as the predominent source of inelastic scattering is incorporated.

An electron transparent sample of silicon in [010] direction with defined thickness steps is prepared by focused ion beam (FIB) (JEOL JIB-4601F, JEOL Ltd.) and polished by low voltage Ar ions using a NanoMill® (Model 1040, E. A. Fischione Instruments). A double aberration-corrected scanning transmission electron microscope JEOL JEM2200FS (JEOL Ltd.) operated at 200 kV and equipped with an in-column omega energy filter above a pixelated detector (pnCCD (S)TEM Camera, PNDetector) allows to obtain energy-filtered CBEDs for every probe position. In addition to unfiltered CBEDs, CBED patterns filtered with an energy window from -5 to 5 eV (elastically scattered) and with an energy window from 5 to 85 eV (inelastically scattered) were acquired. By incorporating plasmon scattering into the simulations[4], a modified version of the STEMsalabim software package[5] is applied to simulate the CBED images.

Results

Recorded CBED patterns as well as position-averaged CBED (PACBED) patterns applying no energy filtering (Unfiltered), zero-loss filtering (Elastic) and filtering at energetic positions where only the zero-loss is blocked (Inelastic) shows distinct differences in the behavior of the patterns. Fig. 1(a) illustrates the electron energy loss (EELS) spectrum along with the ranges in which the energy is filtered. The corresponding unfiltered, elastic and inelastic PACBEDs are also shown in Fig. 1(b), Fig. 1(b) and Fig. 1(d), respectively. The intensity in all the images is normalized to the impinging beam so that a comparison with the image simulations is possible. The elastically scattered PACBED contains coherent information like thickness fringes more clearly than the unfiltered PACBED. In addition, Kikuchi lines in the PACBEDs show the existence of coherent scattering in case of inelastic scattering.

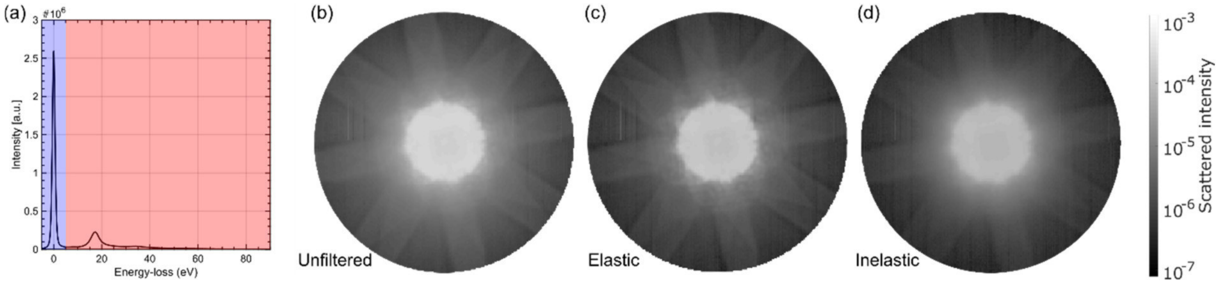

Fig. 1: (a) EELS spectrum of silicon [010] measurement along with the position of the energy slit for the PACBED measurement. (b-d) Corresponding PACBEDs at each energy range illustrated on the EELS spectrum.

Angular dependence of scattering intensity as a function of scattering angle in fractions of the incident beam and normalized to the solid angle of the annular integration regions calculated from unfiltered, elastic, and inelastic PACBEDs (Fig. 1) can be seen in Fig. 2(a). In addition, Fig. 2(b). shows angular dependence of the inelastic to elastic scattering ratio. Inelastic scattering depicts specifically higher intensity at a limited angular range starting from the angles just outside the direct beam. It stresses the importance of considering inelastic scattering for this angular regime. Fig. 2(c) shows the ratio plot for different thickness steps showing thickness dependency of low-loss scattering. As expected, higher sample thickness leads to higher low-loss scattering at all scattering angles. However, the broadening of the ratio peak is not thickness dependent, i. e. the ratio becomes constant at the same scattering angle of around 35 mrad. In addition, at highest thickness (step 6) the ratio within the direct beam is almost the same as the ratio at scattering angles higher than 35 mrad. This trend is changed at lower thicknesses where the ratio within direct beam is lower than the ratio at higher scattering angles.

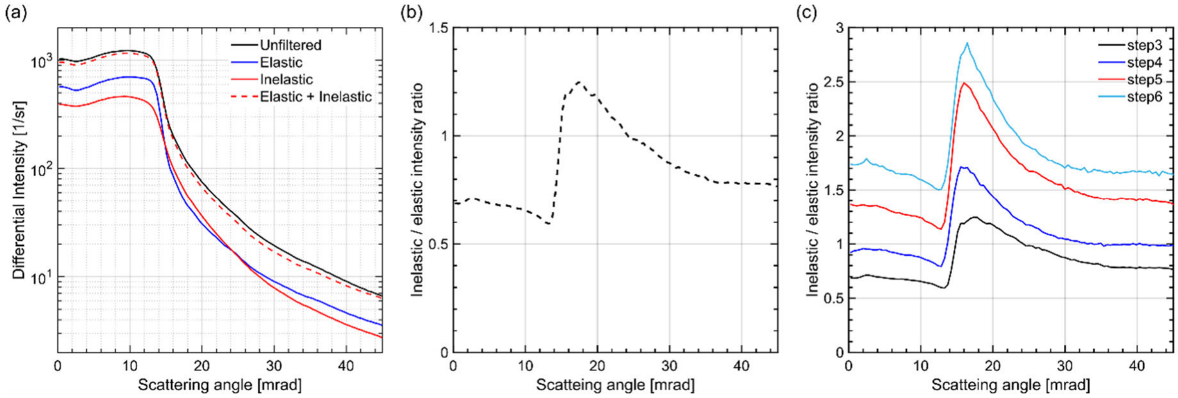

Fig. 2: (a) Angular dependence of scattering intensity as a function of scattering angle in fractions of the incident beam and normalized to the solid angle of the annular integration regions at different energy ranges. (b) Angular dependence of the inelastic to elastic scattering ratio corresponding to the data at panel (a). (c) Inelastic to elastic ratio plot at different thicknesses.

Conclusion

In this work, unfiltered, inelastic as well as zero-loss filtered STEM diffraction patterns are investigated with the example of single crystalline silicon using a fast, pixelated detector. The results highlight features related to inelastic scattering in the angular range outside the direct beam.

Outlook

The same investigation can be applied on different single crystalline materials (e. g. Pt) and binary materials (e. g. GaP) at different orientations. Considering the ability of pixelated detector in recording the complete diffraction pattern at every scanning positon (four dimensional STEM), the effect of energy filtering on synthetic ADF images and COM shift will be investigated for different material systems and different orientations.

Contributing low-loss scattering in the image simulations leads to better matching of simulation and experiments for low angles. It can enable the quantitative evaluation of materials containing light elements (e. g. GaNAs).

References

[1] J. M. LeBeau et al., "Quantitative atomic resolution scanning transmission electron microscopy", Physical Review Letters 100.20 (2008): 206101.
[2] C. C. Lin, and K. Hsu, "Defect Characterization by Differential Phase Contrast Imaging Technique in Scanning Transmission Electron Microscope", in 2019 IEEE 26th International Symposium on Physical and Failure Analysis of Integrated Circuits (IPFA). IEEE. (2019, July): 1-4.
[3] K. Müller-Caspary et al., "Materials characterisation by angle-resolved scanning transmission electron microscopy", Scientific reports 6 (2016): 37146
[4] K. A. Mkhoyan et al., "Critical role of inelastic interactions in quantitative electron microscopy", Physical Review Letters 100.2 (2008): 025503.
[5] J. O. Oelerich et al., "STEMsalabim: A high-performance computing cluster friendly code for scanning transmission electron microscopy image simulations of thin specimens", Ultramicroscopy 177 (2017): 91-96.

Synthesis and Reactivity of Organotetrel Chalcogenide Clusters

K. Hanau,[a] S. Schwan,[b] M. R. Schäfer,[b] M. J. Müller,[c] C. Dues,[d] S. Sanna,[d]
S. Chatterjee,[c] D. Mollenhauer,[b] S. Dehnen[a]

[a] Department of Chemistry and Material Sciences Center, Philipps-Universität Marburg
[b] Institute of Physical Chemistry and Center for Materials Research (LaMa),
Justus-Liebig-Universität Gießen
[c] Institute of Experimental Physics I and Center for Materials Research (LaMa),
Justus-Liebig-Universität Gießen
[d] Institut für Theoretische Physik and Center for Materials Research (LaMa),
Justus-Liebig-Universität Gießen

Introduction

Preliminary work in our group has shown that the structure of tetrel sulfide clusters (heteroadmantane vs. double-decker vs. defect-heterocubane vs. bis-defect-heterocubane) and their properties are influenced by the choice of the elements as well as the organic moiety.[1-3] The adamantane-type cluster $[(StySn)_4S_6]$ (Sty = 4-vinylphenyl) is of special interest, as it shows extreme nonlinear optical properties and acts as an optically active medium in a highly directional visible light emitter driven by a continuous wave laser diode.[4] Furthermore, the organic moieties and the cluster core could be modified in subsequent reactions. An example of this is the reaction of the organo-functionalized tetrel chalcogenide clusters with transition metal complexes, such as $[Cu(PPh_3)_3Cl]$, which leads to the rearrangement of the cluster core and the formation of larger organo-functionalized clusters with a ternary TM/Sn/E core (TM = transition metal, E = chalcogenide).[5-7]

Results

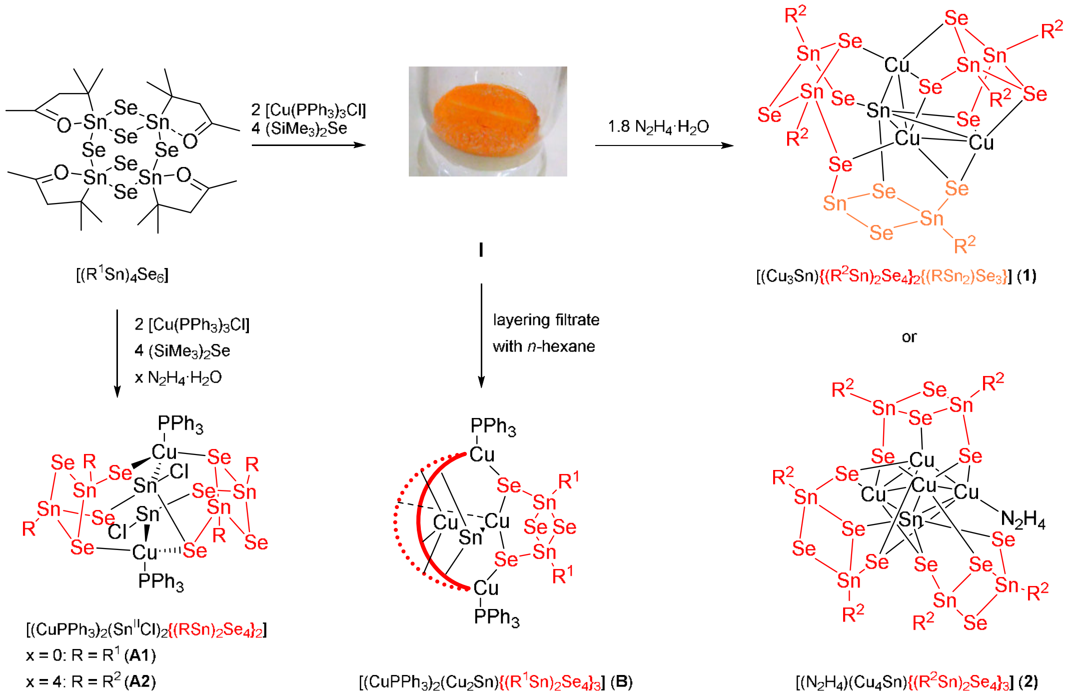

*Scheme 1: Overview of the reactions starting out from $[(R^1Sn)_4Se_6]$, and yielding the new ternary (RSn)/Cu/Se clusters **1** and **2**, as well as the previously reported clusters **A1**, **A2**, and **B** under slightly different reaction conditions (two of the three $\{(R^1Sn)_2Se_4\}$ units are given in a simplified manner in the structural diagram of **B** for the sake of clarity). For details of the synthesis of A1, A2, and B, see refs. [8] and [9]. The $\{(RSn)_2Se_4\}$ building units are highlighted in red; the related $\{(RSn)_2Se_3\}$ unit, which is one Se atom and one organic group short, is drawn in orange.*

We report the formation and structures of two new organotin-copper selenide clusters that were obtained in a two-step procedure.[8] First, $[(R^1Sn)_4Se_6]$ is reacted with $[Cu(PPh_3)_3Cl]$ and $(SiMe_3)_2Se$ to form a bright orange powder (**I**), the nature of which could not be identified in detail; yet a suspension of it in CH_2Cl_2 reacts with $N_2H_4 \cdot H_2O$ to afford single crystals of two cluster compounds, either $[(Cu_3Sn)\{(R^2Sn)_2Se_4\}_2\{(R^2Sn_2)Se_3\}]$ (**1**) ($R^2 = CMe_2CH_2C(NNH_2)Me$) or $[(N_2H_4)(Cu_4Sn)\{(R_2Sn)_2Se_4\}_3]$ (**2**), respectively. Both are based on an intermetallic Cu_xSn cluster core (x = 3, 4), which is surrounded by organotin selenide units $\{(RSn)_2Se_4\}$, $\{(RSn)SnSe_3\}$, or newly $\{(RSn)SnSe_4\}$. The two clusters are structurally related to a series of known clusters, which were obtained under similar reaction conditions, yet from lower concentrations of reactants.[6,7] These reactions are summarized in Scheme 1.

Furthermore, the $[(RSi)_4S_6]$ adamantane-type clusters we reported on last year (R = Sty, R = Np = 1-Naphthyl) were investigated regarding their reactivity towards $[AuCl(PPh_3)]$, their structures, and their optical properties by a combination of comprehensive experimental and theoretical studies.[9] The crystalline compound $[(NpSi)_4S_6]$ shows a pronounced nonlinear optical response, i. e., second-harmonic generation, while for the amorphous $[(StySi)_4S_6]$, the chemical damage threshold so far seems to inhibit a corresponding observation that can clearly put down to nonlinear optical effects. The experimental findings were corroborated by static and time-dependent DFT calculations of both the molecules and the crystalline material, which are in full agreement with the measurements and therefore indicate the applicability of the used methods and models. The observation that clusters with the combination Ph/Si/S and Np/Si/S are crystalline, while the Sn homologues are amorphous was studied on the bases of cluster dimer models calculated with DFT methods. Different types of intra-cluster interactions were found, that led to different dissociation energies as a function of the nature of the substituents, their relative orientation, and the core compositions $\{Si_4S_6\}$ versus $\{Sn_4S_6\}$.

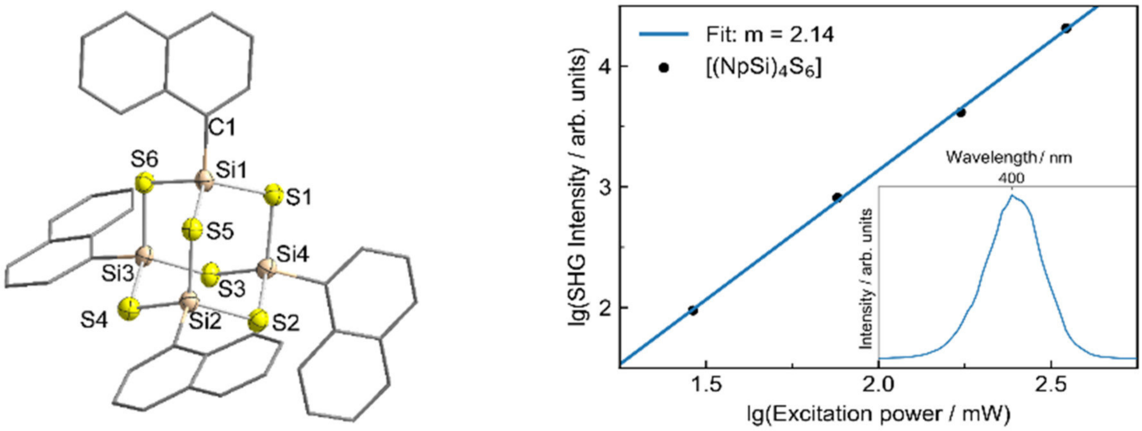

Fig. 1: Molecular structure of $[(NpSi)_4S_6]$ (left) and its nonlinear optical response (right). Excitation power dependency of SHG. SHG spectrum from excitation at 800 nm (inset).

Conclusions

Two new organo-functionalized Cu/Sn/Se clusters were synthesized, adding to the number of such clusters obtained under similar conditions. The results demonstrate the subtle influence of all parameters in the reaction space of such cluster systems, which apparently features a very flat energy hypersurface.

The investigations into adamantane-type Si/S clusters contributed to characterize and further understand the chemical behavior of such clusters, which showed to behave differently from the much better known germanium and tin homologues, and indicates a much more pronounced tendency to polymerization in case of [$(\mathrm{StySi})_4\mathrm{S}_6$] than observed for its Sn homologue, and it confirmed the expected, much higher air- and water sensibility of the Si compounds.

References

[1] Z. Hassanzadeh Fard, L. Xiong, C. Müller, M. Holynska, S. Dehnen, *Chem. Eur. J.* **2009**, *15*, 6595-6604.

[2] J. P. Eußner, B. E. K. Barth, E. Leusmann, Z. You, N. Rinn, S. Dehnen, *Chem. Eur. J.* **2013**, *19*, 13792-13802.

[3] B. Peters, N. Lichtenberger, E. Dornsiepen, S. Dehnen, *Chem. Sci.* **2020**, *11*, 16−26.

[4] N. W. Rosemann, J. P. Eußner, A. Beyer, S. W. Koch, K. Volz, S. Dehnen, S. Chatterjee, *Science* **2016**, *352*, 1301-1304.

[5] E. Dornsiepen, E. Geringer, N. Rinn, S. Dehnen, *Coord. Chem. Rev.* **2019**, *380*, 136-169.

[6] N. Rinn, J. P. Eußner, W. Kaschuba, X. Xie, S. Dehnen, *Chem. Eur. J.* **2016**, *22*, 3094-3104.

[7] N. Rinn, L. Guggolz, J. Lange, S. Chatterjee, T. Block, R. Pöttgen, S. Dehnen, *Chem. Eur. J.* **2018**, *24*, 5840-5848.

[8] K. Hanau, N. Rinn, S. Dehnen, *Inorg. Chem.* **2020**, *59*, 198-202.

[9] K. Hanau, S. Schwan, M. R. Schäfer, M. J. Müller, C. Dues, S. Sanna, S. Chatterjee, D. Mollenhauer, S. Dehnen, *manuscript in preparation.*

Investigation of the reaction of benzylazide on functionalized Si(001) by means of XPS

Julian Heep[1], Christian Länger[1], Jannick Meinecke[2], Ulrich Koert[2], and Michael Dürr[1]

[1]Institut für Angewandte Physik, Justus-Liebig-Universität Gießen
[2]Fachbereich Chemie, Phillips-Universität Marburg

Introduction

The formation of well-ordered structures of organic molecules on semiconductor surfaces, in particular on the technologically most important Si(001) surface, is of great interest both with respect to potential applications as well as from a fundamental point of view. A promising reaction to achieve well-defined layer-growth on silicon is alkyne-azide-coupling[1]. For the semiconductor-organic interface, chemoselective adsorption of an alkyne functionalized cyclooctyne has been previously shown[2]. Benzylazide and its reaction on Si(001) was also investigated intensively by means of XPS, STM, and DFT[3] thus helping with the interpretation of the results in this work, in which we focus on the reaction of benzylazide on an alkyne-substituted cyclooctyne, i. e., ethynyl-cyclopropyl-cyclooctyne (ECCO), the latter being covalently bound to the Si(001) substrate via the strained triple bond of cyclooctyne.

Results

XPS and STM investigations confirmed the selective nature of the reaction of ECCO on Si(001) via the strained triple bond of the cyclooctyne functionality. In order to detect a nitrogen signal in the XPS spectra after exposure of the ECCO-covered Si(001) surface to benzylazide at room temperature, we had to use doses a hundred times higher than what is needed for the adsorption of a monolayer of benzylazide on Si(001). Even then, only a small signal was detected at a binding energy of 398 eV, indicating bond formation between nitrogen and the silicon surface. These results demonstrate that the ECCO layer is tightly packed thus preventing most of the benzylazide molecules from reaching the silicon surface and further reaction with the silicon surface atoms.

When heating the sample to approx. 400 K during dosing the benzylazide, a dose approx. 1000 times higher than the dose applied for saturation coverage on the bare substrate led to the detection of an N 1s signal in the XPS spectra at a binding energy of approx. 400 eV. The latter could be assigned to the benzylazide being reacted with the alkyne group of ECCO. The results demonstrate that alkyne-azide-coupling on the ECCO-functionalized silicon surface is possible. However, the reactivity is low as the reaction typically proceeds in the presence of a catalyst when performed in solution, different to the catalyst-free approach in ultra-high vacuum (UHV) as investigated in this experiment.

Conclusion

It was shown that at high coverage ECCO forms a dense monolayer on Si(001) thus passivating the silicon dimers but leaving the alkyne groups intact for further reaction. Alkyne-azide-coupling was demonstrated, but the reactivity was shown to be comparably low due to the catalyst-free reaction scheme employed under UHV conditions.

Outlook

To achieve a dense second layer of benzylazide on the ECCO-functionalized Si surface via alkyne-azide-coupling, either the molecular dose or the reactivity has to be increased. Both can be realized when transferring the ECCO-functionalized Si samples into solution for the second-layer reaction.

References

[1] N. Münster, P. Nikodemiak, and U. Koert, Org. Lett. **18**, 4296 (2016).
[2] C. Länger, J. Heep, P. Nikodemiak, T. Bohamud, P. Kirsten, U. Höfer, U. Koert and M. Dürr, J. Phys.: Condens. Matter **31**, 034001 (2019).
[3] J. Heep, J.-N. Luy, C. Länger, J. Meinecke, U. Koert, R. Tonner, and M. Dürr, J. Phys. Chem. C **124**, 18, 9940 (2020).

Measuring Atomic Bonding Effects by Combining STEM Multislice Simulations and 4D STEM

Damien Heimes, Jürgen Belz, Andreas Beyer and Kerstin Volz

Department of Physics and Material Sciences Center, Philipps-Universität Marburg

The efficiency of electronic devices is strongly influenced by the dynamical properties of charge carriers and hence by electric fields forming at crystal defects. This makes a decent understanding and characterization of materials on an atomic scale including atomic bonding effects necessary.

Since the electron beam in scanning transmission electron microscopy (STEM) has a diameter in the sub-Angstrom range and is deflected by electric fields present in a sample, STEM is a suitable technique for this task.

The momentum transfer to the electron beam induced by electric fields is proportional to the center of mass (COM) shift in the electron diffraction pattern[1, 2]. By utilizing fast pixelated detectors, the whole diffraction pattern is accessible and the measurement of electric fields and charge redistributions in TEM specimen via STEM becomes possible[3, 4]. The usage of pixelated detectors in STEM is called 4D STEM because to the 2 spatial dimensions of the probe positions the 2 dimensions in the diffraction pattern are added.

A COM shift is no direct prove for the existence of an electric field because many more effects can cause a shift in COM. STEM multislice simulations allow to keep everything except one quantity fixed. Varying only one single quantity at a time makes it possible to investigate the influence of different factors on the COM shift.

Our first exemplary study will be to use STEM simulations[5, 6] to investigate the anti-phase boundary (APB) crystal defect in gallium phosphide (GaP). This defect appears e. g. when GaP is grown on a silicon substrate[7]. Fig. 1 shows how APBs are formed: monoatomic steps in the Si substrate lead to a change of polarity in the GaP, which leads to the formation of charged wrong bonds of Ga-Ga and P-P at the APB[7], highlighted in red.

Fig. 2 shows results from simulations with the STEMsalabim code[6] where the shift in COM in the y-direction for one cubic unit cell of GaP is illustrated. As expected, the COM is shifted towards the atoms.

The influence of charged wrong bonds on the COM will be investigated by comparing STEM simulations with different kinds of atomic scattering potentials: on the one hand potentials from the isolated atoms (IA) approach, which neglect atomic bonding, and on the other hand potentials calculated with density functional theory (DFT), which include atomic bonding. The potentials for both cases are calculated with the GPAW DFT code[8], as it was done in [9].

Fig. 3 shows a comparison of IA potentials and potentials including bonding. Illustrated is the potential of a GaP unit cell, and linescans through it. Linescan a) goes over gallium atoms and shows that on this big scale the potentials do not differ much. The differences between the potentials are revealed by linescans b) and c), which both lie in between atoms. It is clearly visible that the IA potentials are greater than the ones including bonding, which is in accordance with literature[9]. This is due to the fact that the main influence of the electron density is its screening of the atomic potential.

This study shall show that by combining STEM simulations applying DFT potentials and 4D STEM the measurement of charge redistribution due to interatomic bonding is possible and that this enables us to measure the charges at wrong bond defects.

References

[1] K. Müller et al., Nature communications 5.1 (2014): 1-8.
[2] K. Müller-Caspary et al., Ultramicroscopy 178 (2017): 62-80.
[3] N. Shibata et al., Nature communications 8.1 (2017): 1-7.
[4] W. Gao et al., Nature 575.7783 (2019): 480-484.
[5] E. J. Kirkland in “Advanced computing in electron microscopy”, Springer Science & Business Media, 2010.
[6] J. O. Oelerich et al., Ultramicroscopy 177 (2017): 91-96.
[7] A. Beyer et al., Applied Physics Letters 103.3 (2013): 032107.
[8] J. E. Enkovaara et al., Journal of Physics: Condensed Matter 22.25 (2010): 253202.
[9] T. Susi et al., Ultramicroscopy 197 (2019): 16-22.

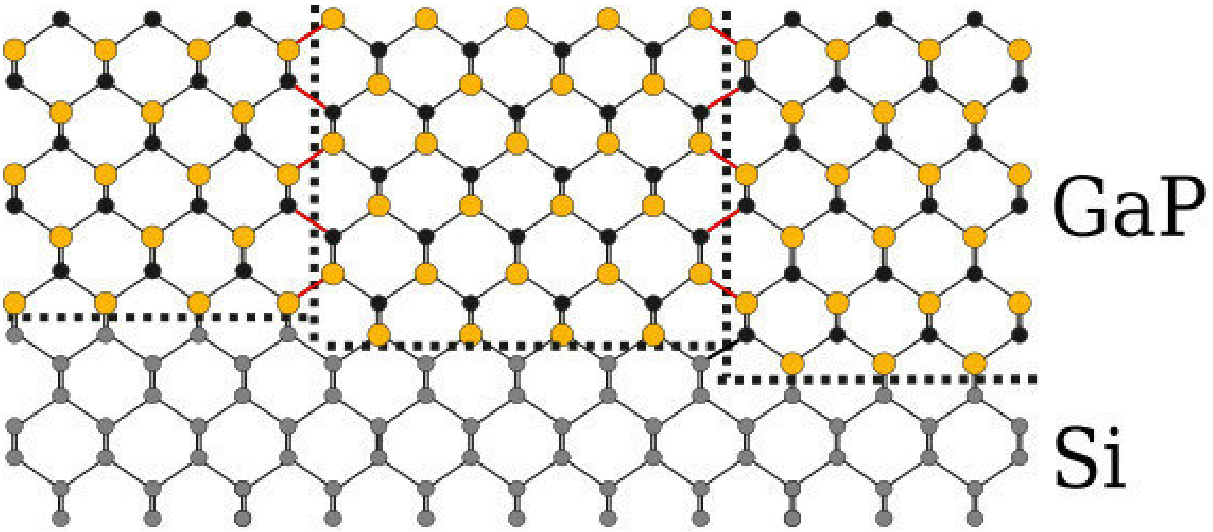

Fig. 1: GaP grown on top of a Si substrate. The monoatomic steps in the substrate lead to the formation of APBs in the GaP, indicated by vertical dashed lines. The charged wrong bonds forming at the APBs are shown in red.

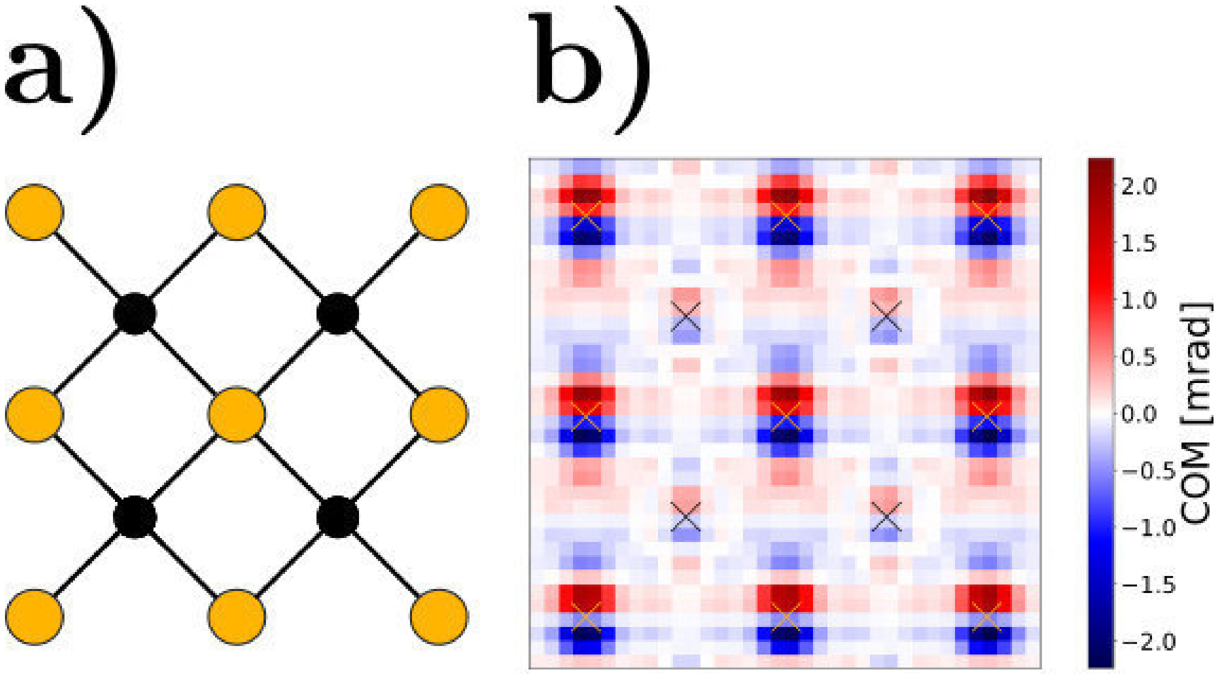

Fig. 2: a) GaP unit cell, with P atoms shown in black and Ga atoms in orange.
b) COM in y-direction for the unit cell in a). Crosses depict the atomic positions.

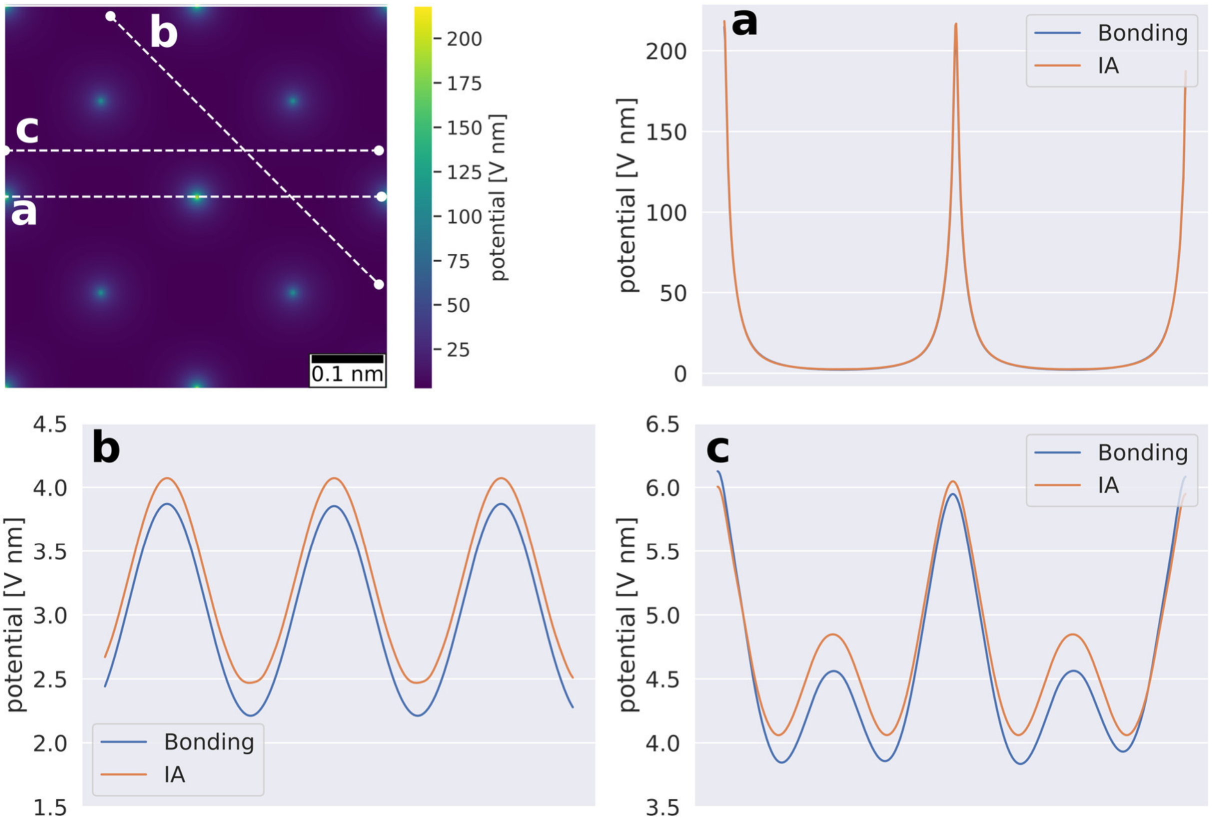

Fig. 3: Atomic potentials for a GaP unit cell as illustrated in Figure 2 a), with linescans over atomic positions (a) and in between atoms (b, c).

Theoretical investigation of azulene and naphthalene on Si(001)

Florian Kreuter

Institute for Physical and Theoretical Chemistry,
Faculty of Chemistry and Pharmacy, University Regensburg

Introduction

In material science, the Si(001) surface is one of the most investigated surfaces due to its interesting electronic properties. The surface is ideal for organic functionalization for its high reactivity caused by the buckled-dimer reconstruction.[1] The upper Si dimer atom is nucleophile, whereas the Si dimer atom is electrophile.[2] Thus, the Si(001) surface can react with nucleophilic as well as electrophilic molecules. Therefore, many studies investigated the adsorption of organic molecules on Si(001).[3] In our group, the adsorption of a diverse set of organic adsorbates on Si(001) has been extensively investigated.[4-8]

One specifically interesting organic molecule is azulene due to its unusually large dipole moment. The adsorption of azulene has been computationally extensively investigated on metallic surface in collaboration with the experimental studies conducted in the Gottfried group.[9-12] These studies show that the interaction between azulene and metal surfaces are particularly strong due to its non-alternating aromatic structure. But up to now, it remains open if azulene also shows unusual reactivity on Si(001) – neither experimental nor computational studies are available.

This study therefore aims to investigate the adsorption of azulene on Si(001). In addition, the alternating-aromatic isomer naphthalene will be investigated as has been done for the metal surfaces before.[9-12] The influence of aromaticity on the adsorption can be studied by comparing the results of azulene and naphthalene on Si(001).

Methods

All investigations are carried out applying density functional theory (DFT). First, the optimized atomic structure of both molecules on the surface are determined. To this end, different starting structures need to be generated and optimized with the help of the program package VASP.[13] Next, the bonding energy of different structures are compared and analyzed. In addition to the structures hand-picked by “chemical intuition”, an unbiased optimization scheme by ab initio molecular dynamic simulations (AIMD) will be used to check that interesting structures are not overlooked. In AIMD, thermally excited movement of the azulene and naphthalene on Si(001) surface are simulated. If the simulated time is long enough, the molecule should run through all possible conformers of the adsorption product. Several trajectories will be run on a supercomputer to ensure that different adsorption pathways are found.

Finally, the character of the molecule-surface bond will be analysed. To this end, the energy decomposition analysis for extended systems (pEDA)[14] is used, which has been developed in the group. In pEDA, the bonding energy is divided into several physically well-defined terms, which make it easier to interpret the bonding character. Also, the system is split in fragments which interact for building the bonds. The first term is the preparation energy. This term describes the energy that is need for deforming the fragments from their ground state structure to the structure in the system. Further pEDA terms are the electrostatic contribution (quasiclassical electrostatic interaction between densities of the two fragments), Pauli repulsion and orbital contribution.

An additional term, which is highly relevant for surface adsorption is dispersion interaction, which is not captured by standard density functionals. In this project, the DFT-D3 method by Grimme et al. is applied to derive the dispersion energies.[15,16]

Results

We are currently investigating the AIMD trajectories for azulene and naphthalene. The adsorption structure of azulene on Si(001) is already obtained by DFT-based optimization based on trial configurations. This structure is shown in the Fig. 1, where can be seen that azulene is strongly deformed by adsorption on the surface. Azulene is not planar anymore but shows strong bending. The deformation is a sign of covalent bonding interaction between azulene and Si(001) surface. Furthermore, azulene seems to form four C-Si-bonds with the surface, which is also shown in Fig. 1. The strong interaction between azulene and Si(001) surface is consistent with high bonding energy (-243 kJ mol^{-1}). The contribution from dispersion interaction to the bonding energy amounts to 71 kJ mol^{-1} (29 % of the total bonding energy). The pEDA calculation for azulene using two closed shell fragments shows that the preparation energy and the orbital contribution are very large. It could be an indicator that the closed-shell fragmentation (donor-acceptor bond picture) needs to be questioned and open-shell fragmentation is currently underway (shared-electron bond picture). Furthermore, the four C-Si-bonds indicate that a quintet fragmentation could be the better choice.

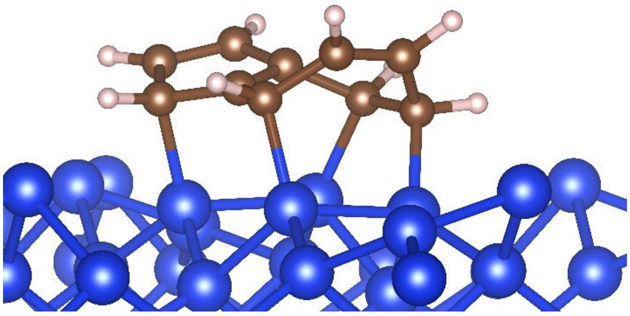

Fig. 1: Stucture of azulene on Si(001)

Outlook

The plan for the next time is to finish all running calculation and to analyze result. The goal is to obtain an intuitive picture of adsorption of azulene and naphthalene on Si(001) surface. Also, the influence of aromaticity on adsorption will be investigated. We will also compare the results to our previous investigations on metal surfaces.

References

[1] R. E. Schlier, H. E. Farnsworth, *The Journal of Chemical Physics* **1959**, *30*, 917.

[2] J. Yoshinobu, *Progress in Surface Science* **2004**, *77*, 37.

[3] A. V. Teplyakov, S. F. Bent, *Journal of Vacuum Science & Technology A: Vacuum, Surfaces, and Films* **2013**, *31*, 50810.

[4] J. Pecher, G. Mette, M. Dürr, R. Tonner, *Chemphyschem: A European journal of chemical physics and physical chemistry* **2017**, *18*, 357.

[5] J. Pecher, R. Tonner, *Chemphyschem: A European journal of chemical physics and physical chemistry* **2017**, *18*, 34.
[6] L. Pecher, S. Laref, M. Raupach, R. Tonner, *Angewandte Chemie (International Ed. in English)* **2017**, *56*, 15150.
[7] L. Pecher, S. Schmidt, R. Tonner, *J. Phys. Chem. C* **2017**, *121*, 26840.
[8] L. Pecher, C. Schober, R. Tonner, *Chemistry (Weinheim an der Bergstraße, Germany)* **2017**, *23*, 5459.
[9] S. R. Kachel, B. P. Klein, J. M. Morbec, M. Schöniger, M. Hutter, M. Schmid, P. Kratzer, B. Meyer, R. Tonner, J. M. Gottfried, *J. Phys. Chem. C* **2020**, *124*, 8257.
[10] B. P. Klein, S. E. Harman, L. Ruppenthal, G. M. Ruehl, S. J. Hall, S. J. Carey, J. Herritsch, M. Schmid, R. J. Maurer, R. Tonner et al., *Chem. Mater.* **2020**, *32*, 1041.
[11] B. P. Klein, J. M. Morbec, M. Franke, K. K. Greulich, M. Sachs, S. Parhizkar, F. C. Bocquet, M. Schmid, S. J. Hall, R. J. Maurer et al., *J. Phys. Chem. C* **2019**, *123*, 29219.
[12] B. P. Klein, N. J. van der Heijden, S. R. Kachel, M. Franke, C. K. Krug, K. K. Greulich, L. Ruppenthal, P. Müller, P. Rosenow, S. Parhizkar et al., *Phys. Rev. X* **2019**, *9*.
[13] a) G. Kresse, J. Hafner, Phys. Rev. B 1993, 47, 558; b) G. Kresse, J. Hafner, *Phys. Rev. B* **1994**, *49*, 14251; c) G. Kresse, J. Furthmüller, *Phys. Rev. B* **1996**, *54*, 11169; d) G. Kresse, J. Furthmüller, *Comput. Mater. Sci.* **1996**, *6*, 15.
[14] M. Raupach, R. Tonner, *The Journal of Chemical Physics* **2015**, *142*, 194105.
[15] S. Grimme, J. Antony, S. Ehrlich, H. Krieg, *The Journal of Chemical Physics* **2010**, *132*, 154104.
[16] S. Grimme, S. Ehrlich, L. Goerigk, *Journal of computational chemistry* **2011**, *32*, 1456.

Optische Spektroskopie an Organisch-Anorganischen Hybridstrukturen – Ladungstransfer an der Grenzfläche von Farbstoffsolarzellen

Meyenburg*, N. Hofeditz*, J. Falgenhauer**, D. Schlettwein**, W. Heimbrodt*

*Fachbereich Physik und WZMW, Philipps-Universität Marburg**
*Institut für Angewandte Physik, Justus-Liebig-Universität Gießen***

Die Funktionalisierung von anorganischen Halbleitern mit organischen Schichten ist ein hochaktuelles Forschungsfeld in der Halbleiterphysik. Organisch-anorganische Halbleiter-Hybride sind vielversprechende Funktionsmaterialien für innovative optoelektronische Bauelemente, beispielsweise für Farbstoff-Solarzellen vom Typ Grätzel. Ein wichtiger Prozess bei hocheffizienten Grätzel-Solarzellen ist eine optimierte Elektronenübertragung von den Exzitonen des adsorbierten Farbstoffes in den anorganischen Halbleiter an der Hybrid-Grenzfläche. Wir untersuchten daher die elektronischen und optoelektronischen Wechselwirkungen organisch-anorganischer Halbleitersysteme mittels optischer Spektroskopie.

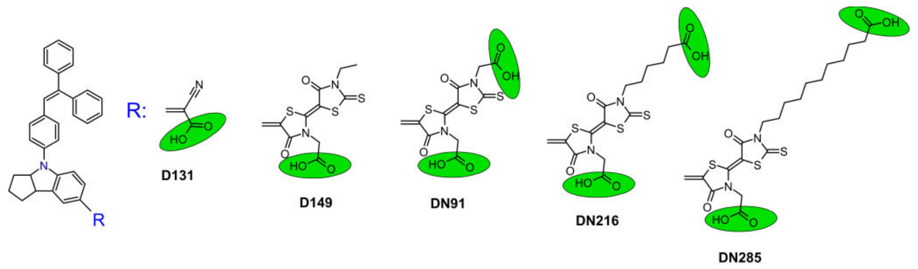

Abb. 1: Schematische Darstellung der chemischen Struktur der verschiedenen Indolin-Derivate.

Die untersuchten Hybride bestehen aus Indolinderivaten (Abb. 1) und unterschiedlichen anorganischen Substraten (TiO_2, ZnO, SiO_2 (0001), Quarzglas). Wir ermitteln die Elektron-Transferzeiten durch Analyse der Photolumineszenz-Transienten des Farbstoffes nach Femtosekundenanregung mittels Anwendung von kinetischen Modellrechnungen[1]. Ein Elektronentransfer tritt als Verlustkanal des angeregten Farbstoffes auf, die Verlaufskurve der Photolumineszenz des Farbstoffes klingt dadurch bei Transfer schneller ab als ohne Transfer auf Glas (Abb. 3).

Die relevanten Prozesse, nämlich Anregung, Rekombination, Diffusion und Ladungstransfer sind schematisch in Abb. 2 dargestellt.

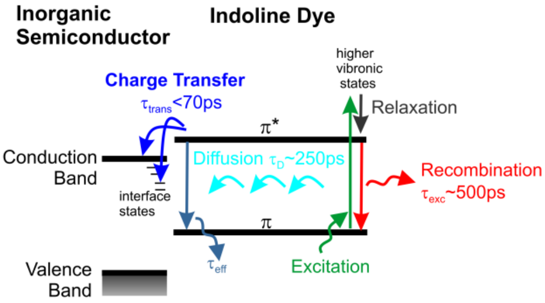

Abb. 2: Schematische Darstellung der Prozesse an der Schnittstelle zwischen Leitungsschicht und anorganischem Halbleiter.

Es wurde eine Korrelation zwischen den Übertragungszeiten und vier Parametern gefunden: (i) Anzahl der Ankergruppen, (ii) der Abstand zwischen dem Farbstoff und der organisch-anorganischen Grenzfläche, welcher durch die Alkylkettenlängen zwischen der Carboxylat-

Ankergruppe und dem Farbstoff variiert wurde, (iii) die Dicke der adsorbierten Farbstoffschicht und (iv) der Energieniveau-Unterschied zwischen dem angeregten Farbstoff (π*-Niveau) und dem Leitungsbandminimum des anorganischen Halbleiters.

Der Vergleich von D149 und DN91 zeigt, dass der zweite COOH-Anker und die damit erwartete stärkere Anbindung die Ladungsübertragung verbessert. Wird der Abstand zwischen dem Chromophor und der Grenzfläche durch Verlängerung der Ankerkette vergrößert (DN91 → DN216 → DN285), so reduziert sich die Transferwahrscheinlichkeit. Der schnellste Transfer wurde für die D131 gefunden (Abb. 4). Dies wird auf größere Energieunterschiede zwischen dem Zustand des angeregten Farbstoffs und des Leitungsbandes des Bulk-Halbleiters zurückgeführt.

Optoelektronische Messungen zeigen die Änderungen der Elektronentransferzeiten durch Anlegen einer elektrischen Vorspannung (Abb. 5). Durch Schieben der Fermi-Energie im ZnO-Substrat in Richtung des angeregten Farbstoffniveaus wird die Transferzeit länger[2].

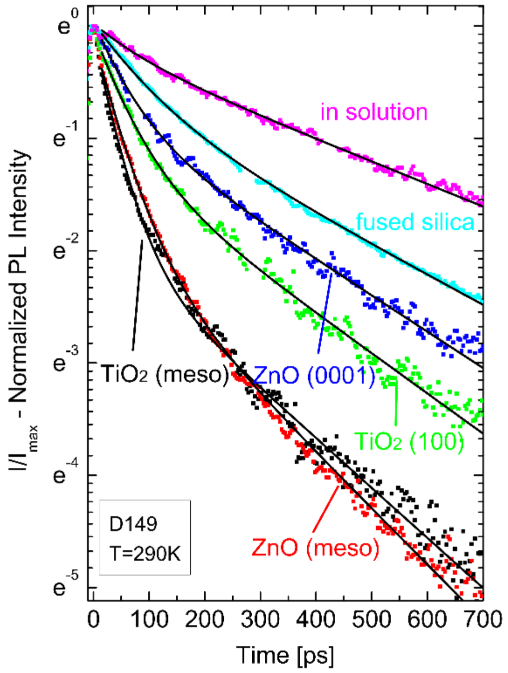

Abb. 3: Photolumineszenz-Abklingkurven von D149 in Lösung und auf verschiedenen Substraten.

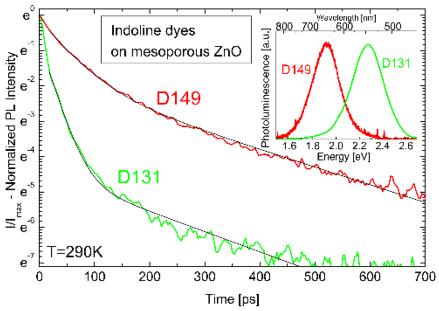

Abb. 4: Photolumineszenz-Abklingkurven von D131 und D149 auf mesoporösem ZnO.
Inset: PL-Spektrum

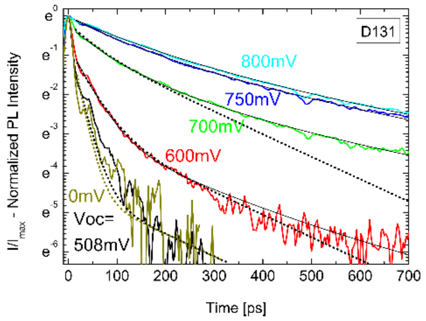

Abb. 5: Photolumineszenz-Abklingkurven von D131 abhängig von der angelegten Spannung

[1] I. Meyenburg, J. Falgenhauer, N. W. Rosemann, S. Chatterjee, D. Schlettwein, W. Heimbrodt (2016). Journal of Applied Physics, 120 (21), 215502.

[2] I. Meyenburg, N. Hofeditz, R. Ruess, M. Rudolph, J. Falgenhauer, D. Schlettwein, W. Heimbrodt (2018). AIP Advances, 8 (5), 055218.

Ionothermal Design of Exfoliable Telluridomercurate Materials

B. Peters and S. Dehnen

Department of Chemistry and Material Sciences Center, Philipps-Universität Marburg

Chalcogenido metalates have been a multi-addressed subject in the last decades, because of their intriguing (semi)conducting properties.[1,2] In addition to several traditional synthesis methods, our group currently sets the focus on ionothermal approaches, which show various advantages: moderate temperatures, high efficiencies and modifiability.[3,4] Furthermore, the method allows fine-tuning of heavy-element structures within metalate materials.[5,6] These issues perfectly qualifies the ionothermal approach for the design and synthesis of nano-structured tellurido-mercurate materials.[7]

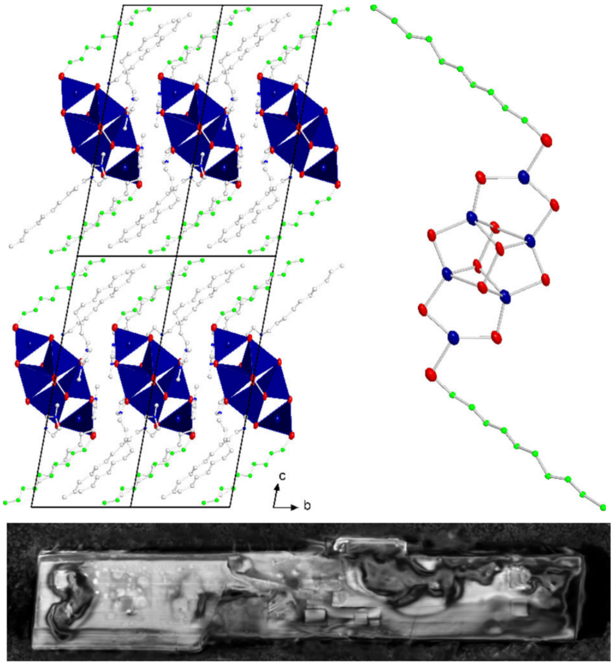

Fig. 1: Top: Super cell of ***1*** *and molecular structure of the* $[Hg_6Te_6(Te_2)_2(Te\text{-}Dec)_2]^{6-}$ *anion; Te: red, Hg: blue; carbon: grey/green, nitrogen: light blue; hydrogen atoms omitted for clarity. Bottom: SEM image of a single-crystal of* ***1****.*

We successfully obtained a novel compound with an unprecedented anionic substructure, $[\mathrm{Cat}]_6[\mathrm{Hg_6Te_6(Te_2)_2(Te\text{-}Dec)_2}]$ (**1**, Fig. 1, top; Dec = decyl, $C_{10}H_{21}$). Imidazolium cations (Cat) act as counterions for compensation of the anions' charge in the solid. The crystal structure of the compound shows a lamellar assembly of alternating layers comprising anions and imidazolium rings besides layers of the unpolar alkyl chains of the imidazolium derivatives. This circumstance is an excellent precondition for the generation of nanostructured sheets via exfoliation.[8] First attempts of exfoliating crystals of **1** were studied by SEM (Fig. 1, bottom).

References

[1] N. Zheng, X. Bu, P. Feng, *Nature* **2003**, *426*, 428–432.

[2] N. Zheng, X. Bu, B. Wang, P. Feng, *Science* **2002**, *298*, 2366–2369.

[3] M. G. Kanatzidis, *Inorg. Chem.* **2017**, *56*, 3158–3173.

[4] S. Santner, J. Heine, S. Dehnen, *Angew. Chem. Int. Ed.* **2016**, *54*, 876-893.

[5] Y. Pei, C. Chang, Z. Wang, M. Yin, M. Wu, G. Tan, H. Wu, Y. Chen, L. Zheng, S. Gong, T. Zhu, X. Zhao, L. Huang, J. He, M. G. Kanatzidis, L.-D. Zhao, *J. Am. Chem. Soc.* **2016**, *138*, 16364−16371.

[6] B. Peters, N. Lichtenberger, E. Dornsiepen, S. Dehnen, *Chem. Sci.* **2020**, *11*, 16−26.

[7] C. Donsbach, K. Reiter, D. Sundholm, F. Weigend, S. Dehnen, *Angew. Chem. Int. Ed.* **2018**, *57*, 8770–8774.

[8] L. Dou, A. B. Wong, Y. Yu, M. Lai, N. Kornienko, S. W. Eaton, A. Fu, C. G. Bischak, J. Ma, T. Ding, N. S. Ginsberg, L.-W. Wang, A. P. Alivisatos, P. Yang, *Science* **2015**, *349*, 1518–1521.

Investigation on Preparation of Interpnictogen Compounds for Possible Application in MOVPE

Christian Ritter, Carsten von Hänisch

Department of Chemistry and Material Sciences Center, Philipps-Universität Marburg

Introduction

Since the DTBAA precursor for growing dilute nitride GaAs semiconductors gained high attention due to significant better N incorporation than state of the art UDMHy the investigation of novel group 15 compounds for possible application in MOVPE come to the fore of interests.[1,2] Therefore especially interpnictogen molecules seems to provide a lot of unexploited potential. For a focused synthesis of novel precursors a fundamental investigation on the reactivity of this class of compounds is crucial. Up to now no molecule is known that contains all group 15 elements from nitrogen to bismuth. Beside the unknown quinternary only two quaternary interpnictogen compounds were prepared until now.[3,4]

Results

The conversion of $AsCl_3$ with an excess of tBuNH$_2$ leads to the *tert*-butyl amido substituted four membered nitrogen arsenic ring (tBuNH)$_2$(AsNtBu)$_2$ (**1**) first described by Vetter *et al.* in 1964.[5] The lithiation and following conversion with $BiCl_3$ and $SbCl_3$ have been published, but only for the corresponding Sb compound sufficient analytical data were provided.[6,7] To this series I added the product of the conversion with $AsCl_3$ yielding compounds (**3**–**5**, Fig. 1) as synthons for further conversions with some binary interpnictogen compounds previously described within our group (tBu$_2$As-P(Li)tBu & tBu$_2$Sb-P(Li)tBu).[8,9]

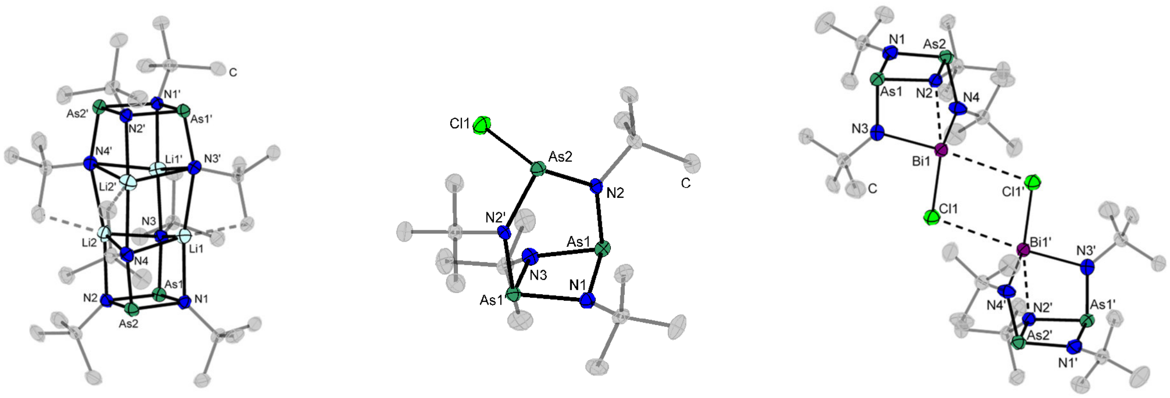

*Fig. 1: Molecular structures in the solid state of **2**, **3** and **5** in the solid state. Hydrogen atoms are omitted for clarity.*

Within the reaction of **3**–**5** with tBu$_2$Sb-P(Li)tBu the desired products were obtained and fully characterized (**6**–**8**, Fig. 2 top). **8** represents the first molecule containing all pnictogens atoms from nitrogen to bismuth. Furthermore it is surprisingly stable against room temperature and light, which is remarkable, since it contains a covalent bismuth phosphorus bond that is known to be very weak. The reason for this relative high stability is probably the chelating coordination from the two bonded nitrogen atoms as well as from one of the nitrogen atoms of the four membered ring with an additional weak interaction. In contrast, the reaction with tBu$_2$As-P(Li)tBu leads to reduction of **3**–**5** instead, yielding the dipnictogenes **9**–**11** (Fig. 2 bottom).

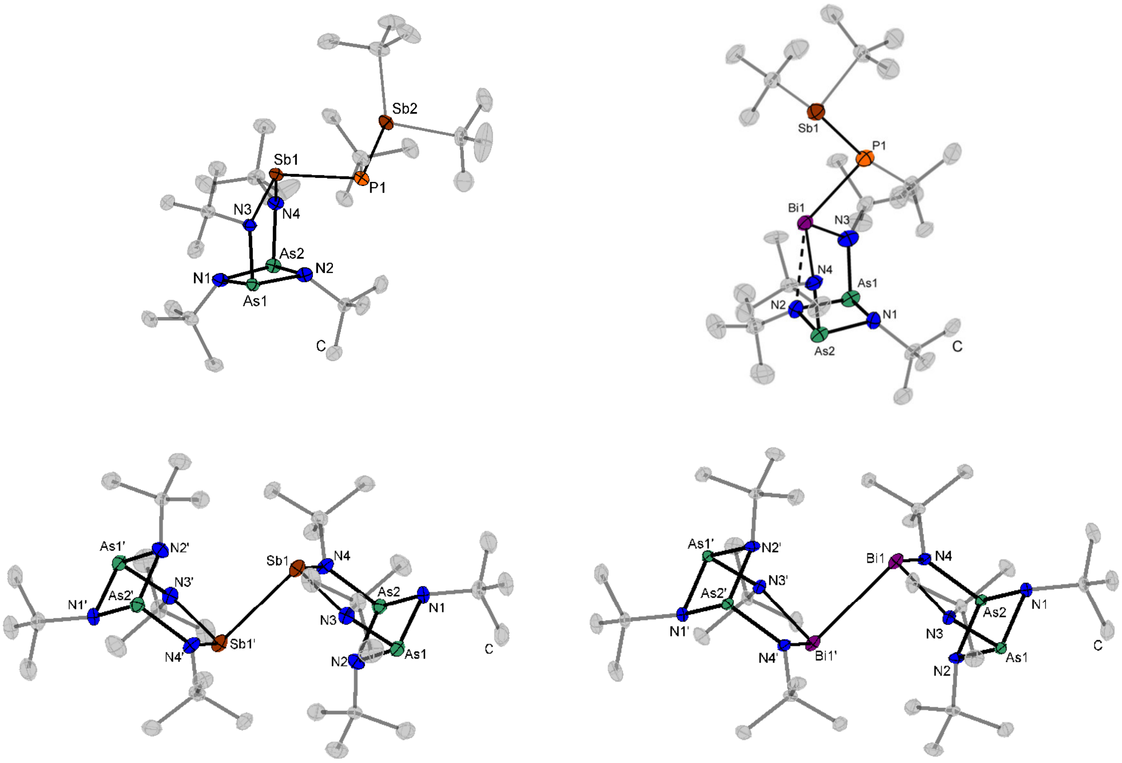

*Fig. 2: Molecular structures in the solid state of **7** & **8** (top) and **10** & **11** (bottom) in the solid state. Hydrogen atoms are omitted for clarity.*

Conclusion and Outlook

Motivated by the promising results of the DTBAA precursor in the MOVPE process we investigated the reactivity of compounds with elements of the group 15 mixed together. We did this to gain insights for future development of novel molecules with possible application as group 15 precursors. Therefore we synthesized two novel quaternary and the first quinternary interpnictogen compound containing all elements from nitrogen to bismuth. Future works will concentrate on preparing other element combinations and orders in this class of compounds. Based on those results we will synthesize novel interpnictogen precursors for future applications.

References

[1] E. Sterzer, A. Beyer, L. Duschek, L. Nattermann, B. Ringler, B. Leube, A. Stegmüller, R. Tonner, C. von Hänisch, W. Stolz, et al., *J. Cryst. Growth* **2016**, *439*, 19-27.
[2] E. Sterzer, B. Ringler, L. Nattermann, A. Beyer, C. von Hänisch, W. Stolz, K. Volz, *J. Cryst. Growth* **2017**, *467*, 132-136.
[3] R. Garbe, S. Wocadlo, H.-C. Kang, W. Massa, K. Harms, K. Dehnicke, *Chem. Ber.* **1996**, *129*, 109-113.
[4] A. Hinz, A. Schulz, A. Villinger, *Chem. Commun.* **2015**, *51*, 11437-11440.
[5] H.-J. Vetter, H. Nöth, W. Jahn, *Z. Anorg. Allg. Chem.* **1964**, *328*, 144-153.
[6] M. Veith, A. Rammo, M. Hans, *Phosphorus. Sulfur. Silicon Relat. Elem.* **1994**, *93*, 197-200.
[7] L. Belter, W. Frank, *Phosphorus Sulfur Relat. Elem.* **2016**, *191*, 675-677.
[8] B. Ringler, M. Müller, C. von Hänisch, *Eur. J. Inorg. Chem.* **2018**, *2018*, 640-646.
[9] C. Ritter, F. Weigend, C. Hänisch, *Chem. Eur. J.* **2020**, *26*, 8536-8540.

Ga(As,Bi)-based Type-II QW and W-Type Heterostructures

J. Veletas[1], T. Hepp[2], K. Volz[2], and S. Chatterjee[1]

[1]Institute of Experimental Physics I, Justus-Liebig-Universität Gießen
[2]Department of Physics and Material Sciences Center, Philipps-Universität Marburg

Introduction

Dilute bismuth-containing semiconductor alloys such as Ga(As,Bi) are attracting significant attention due to their promising characteristics in near- and mid-infrared laser applications. Beside the use as an active medium for telecommunication wavelength lasers, bismuthide semiconductors offer the possibility of lasers with even longer wavelength and, in general, a wide scope for band structure engineering. Additionally, spatially indirect transitions offer the possibility for light emitting devices on the GaAs platform. Such type-II structures can act as active regions in infrared laser structures. For example, Ga(N,As) and Ga(As,Bi) serve as electron QW and hole QW, respectively. We use optical spectroscopy to gain information about the charge-carrier recombination path and the influence between type-II and W-type heterostructures.

Results

Temperature dependent photoluminescence spectroscopy (PL) reveals the particular influence of the electron QW and hole QW on the emission properties. Fig. 1 displays the PL-maxima and the full width at half maximum (FWHM) as a function of the temperature. The upper two plots are data obtained from Ga(As,Bi) and Ga(N,As) type-I reference samples. A direct comparison of symmetric (yellow data) and asymmetric (green data) Ga(N,As)/Ga(As,Bi) type-II quantum well heterostructures reveals that the symmetry of the layer arrangement drastically influences the charge-carrier recombination: disorder in the Ga(As,Bi) layer has more prominent effects for the asymmetric configuration compared to the symmetric one. The emission energy is mainly influenced by the Ga(N,As)-electron quantum wells, while the full width at half maximum is dominated by the Ga(As,Bi)-hole quantum wells. Excitation dependent PL measurements (data not shown here) reveal localized states for the Ga(As,Bi) reference structure, the type-II and the W-type structure. We interpret these localized states as the origin for the differences of the FWHM.

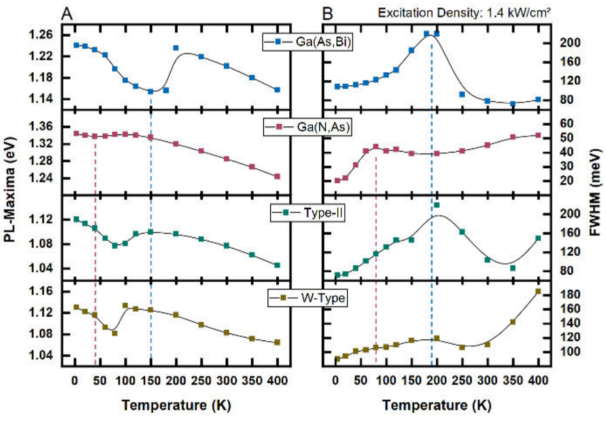

Fig. 1: PL-maxima and FWHM of the investigated structures as a function of the lattice temperature.

Photoluminescence excitation spectroscopy (PLE) data reveal the carrier recombination paths in type-II structures. PLE and PL at a lattice temperature of 4 K data are shown in Fig. 2 for the asymmetric type-II structure (A) and the symmetric W-type structure (B). The dashed vertical line indicates the detection energy for the PLE measurements. While the PL line shapes are quite similar, the PLE spectra of the asymmetric and symmetric structure reveal some distinct differences. Two low-energy peaks originating from the Ga(N,As) and the Ga(As,Bi) layer are expected in addition to the increase for energies above 1.5 eV. However, only one additional peak is observable in the PLE measurements for either of the samples. For the symmetric W-type structure, the low-energy tail of the resonance at 1.35 eV is much steeper and the resonance seems to be sharper supporting the findings of the results discussed above. The “missing peak” suggests that the Ga(As,Bi) layer contributes insignificantly to the recombination via the spatially indirect transition in both cases. The carriers excited in the Ga(As,Bi) layers are mostly trapped in the localized states and, thus, cannot contribute to the type-II transition.

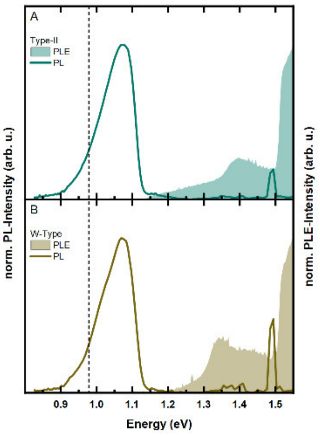

Fig. 2: PLE and PL spectra of the asymmetric type-II and the symmetric W-type structure.

Conclusions

The analysis of the disorder signatures and the carrier recombination paths allows a clear distrinction between the influences of the two species of QWs on the type-II recombination. The specific properties of the type-I reference structures enables an unambiguous assignment of the influence of the layers’ materials properties on the type-II recombination.

Outlook

In terms of device optimization, the dynamical properties are critical quantities. Future experiments will address the opto-dynamical properties. Time-resolved PL spectroscopy gives information on carrier recombination-times and pump-probe spectroscopy provides a deeper understanding on the relaxation mechanisms.

In-situ TEM Growth Investigations of III/V Semiconductor Materials

Maximilian Widemann, David Krug, Andreas Beyer, Kerstin Volz

Department of Physics and Material Sciences Center, Philipps-Universität Marburg

Introduction

III/V semiconductors are used for many technical applications, like for example LEDs, lasers and solar cells. A widely used fabrication process of these materials is metal organic vapor phase epitaxy (MOVPE). However, structural investigations of the samples are usually carried out post growth. *In-situ* studies of the growth process promise an improvement of the fabricated materials performance. But it comes along with several challenges, like the realization of the growth conditions inside a TEM or the incongruent evaporation of the group V compound at elevated temperatures. *In-situ* (scanning) transmission electron microscopy ((S)TEM) allows to investigate dynamic processes, which occur during the thermal annealing or the growth of III/V semiconductor materials inside a TEM. Gas environmental cell and heating holders enable to supply gases while heating the sample, so that conditions comparable to those during the MOVPE process can be realized in any electron microscope[1].

Methods

To this end, a commercially available Protochips *in-situ* system has been modified. In order to allow the usage of toxic and pyrophoric gases, like the precursor gases used in MOVPE growth a gas mixing system, an appropriate gas monitoring system as well as a gas scrubbing system have been added to the setup[2]. To analyze the compounds of the gases and to detect reaction products a SRS 200 amu residual gas analyzer (RGA) has been integrated. A sample preparation technique is necessary, which allows a controlled transfer of a microscopic and electron transparent sample onto a micro electro mechanical system (MEMS) chip of gas environmental cell holder[3]. This is given by the focused ion beam (FIB) lift out technique and is performed in a JEOL JIB-4601F dual beam system. A double C_S-corrected JEOL JEM 2200FS operating at 200 kV is used for the TEM observations. As a model system GaP nanowires (NW) have been investigated in first growth experiments, since their growth observation comes along with less challenges compared to layer growth processes. Precursor gases used for GaP based experiments are tertiarybutylphosphine (TBP) and trimethylgallium (TMGa). Additionally, N_2 can be used as carrier gas.

Obviously, there is a huge geometrical difference between macroscopic bulk samples and microscopic TEM samples, which have a much higher surface to volume ratio. Nevertheless, thermal stability of these samples under elevated temperatures, which are required for annealing or crystal growth, can be achieved like it is done for bulk samples by a surplus of the group V precursor gas[2]. Furthermore the microscopic geometry of the closed cell holder, which acts as MOVPE reactor, is capable of decomposing the precursor gases and grow crystalline materials from gas phase.

NW vapor liquid solid (VLS) growth experiments catalyzed by gold nanoparticles (NP) have been performed with a total pressure of 400 hPa and precursor partial pressures between 10^{-1} hPa and 10^{-3} hPa with a V/III ratio of 10. Growth temperature has been varied between 400 °C and 450 °C.

Results

The experiments demonstrate the influence of the growth parameters on the NW morphology and growth rate. Temperature strongly determines the shape of the NWs. At 450 °C grown samples show a straight growth behavior, whereas NWs grown at 400 °C form many kinks. Measurements of these kinking angles show a predominance of 70° (Fig. 1a). This is most probably caused by twin boundaries (Fig. 1b)[4]. This defect appears on the gallium terminated (111) surfaces[5]. The reason why the 70° angle is formed more often than the 110° angle, which might be caused by this defect as well, may be given by the conservation of the layer formation order, which is assumed to be from gallium to phosphorus. A further frequently observed angle is around 123°. These angles can occur when twins of second order are formed, meaning two twins after another.

The growth rate of the NWs can be controlled mainly by the partial pressures of the precursor gases. Higher partial pressures lead to an increased incorporation of growth material. Another crucial factor for the growth rate is given by the surface ratio of droplet and growth plane. NWs with different surface ratios can be seen in the STEM images in Fig. 2a during the growth at 450 °C and partial pressures of 1.6×10^{-2} hPa (TBP) and 1.8×10^{-3} hPa (TMGa). The wires show a big difference in the surface ratios, resulting in growth rates of 39.9 nm/s and 2.7 nm/s under the same conditions respectively. Since the incorporated material needs to diffuse across the droplet surface through the liquid catalyst, a higher droplet surface leads to more diffusion of the limiting species growth material. Whereas an increased interface area between droplet and growth plane reduces the growth rate. Fig. 2b show the growth rate for 13 different NWs of this experiment in dependence of their surface ratios, indicating a linear proportionality.

Furthermore, we compare the growth of nanowires in post growth investigations with applying the same growth conditions with and without electron beam, respectively. All in all, the electron beam seems to have a negligible influence on nanowire growth under appropriate conditions. This suggests that results, collected in *in-situ* TEM growth investigations, can be transferred to processes appearing in conventional MOVPE growth.

Outlook

In further *in-situ* growth experiments, the detailed dependencies of temperature and precursor partial pressures as well as the catalyst droplet geometry on the growth rate needs to be investigated. Also images and videos of atomic resolved layer formation is still missing. To achieve this, a sample preparation technique is needed to prepare NWs on a substrate, which determines the crystal orientation. Since the closed gas cell holder has only single tilt capabilities, it is only reliable to tilt NWs into zone axis with control over the crystal orientation. Additionally, atomic resolved images of twin boundaries causing the 70° kinking angles are to come. Moreover the insights gained in *in-situ* TEM growth investigations need to be transferred to growth mechanisms like they appear in the MOVPE layer growth. Such experiments require substrate samples in zone axis, which can be achieved by the FIB lift out technique. This promises a deeper understanding of the processes taking place in a MOVPE growth machine, leading to the improvement of grown materials properties.

References

[1] L. F. Allard et al. "A new MEMS-based system for ultra-high-resolution imaging at elevated temperatures." *Microscopy research and technique* 72.3 (2009): 208-215.

[2] R. Straubinger et al. "In Situ Thermal Annealing Transmission Electron Microscopy (TEM) Investigation of III/V Semiconductor Heterostructures Using a Setup for Safe Usage of Toxic and Pyrophoric Gases." *Microscopy and Microanalysis* 23.4 (2017): 751-757.

[3] R. Straubinger, A. Beyer, and K. Volz. "Preparation and loading process of single crystalline samples into a gas environmental cell holder for in situ atomic resolution scanning transmission electron microscopic observation." *Microscopy and Microanalysis* 22.3 (2016): 515-519.

[4] M. Zhang, et al. "Formation mechanisms for the dominant kinks with different angles in InP nanowires." *Nanoscale research letters* 9.1 (2014): 211.

[5] A. Beyer, et al. "Influence of crystal polarity on crystal defects in GaP grown on exact Si (001)." *Journal of Applied Physics* 109.8 (2011): 083529.

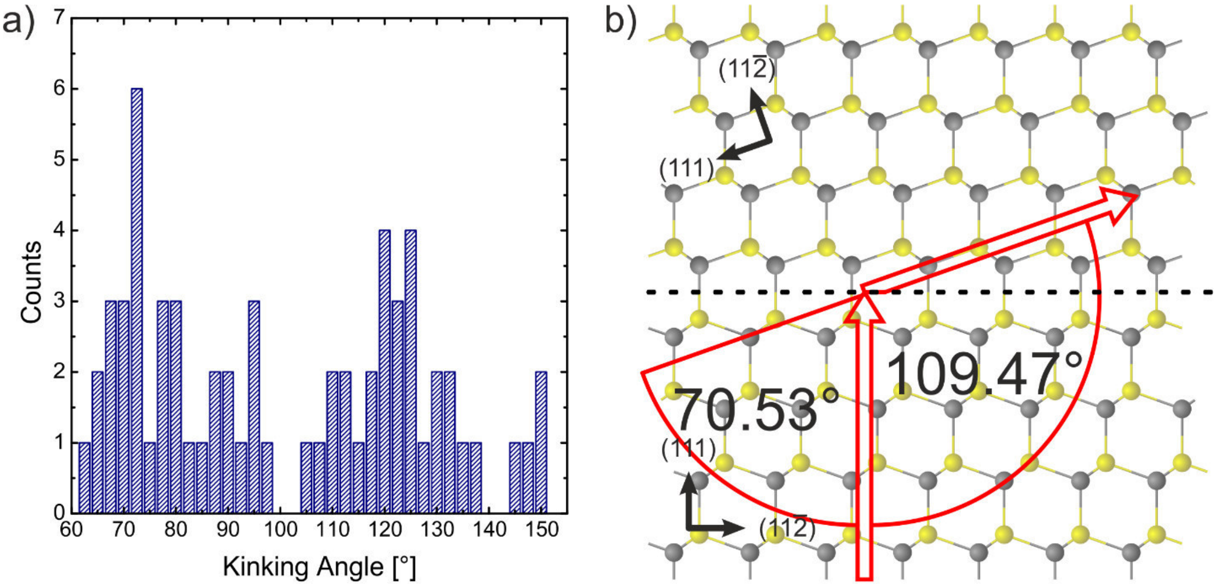

Fig. 1 a) Histogram of kinking angles of NWs grown at 400 °C. The predominance of 70°, 110° and 123° indicates twin boundary defects causing these kinks. b) Schematic drawing of a twin boundary (black line) in [1$\bar{1}$ 0] projection.

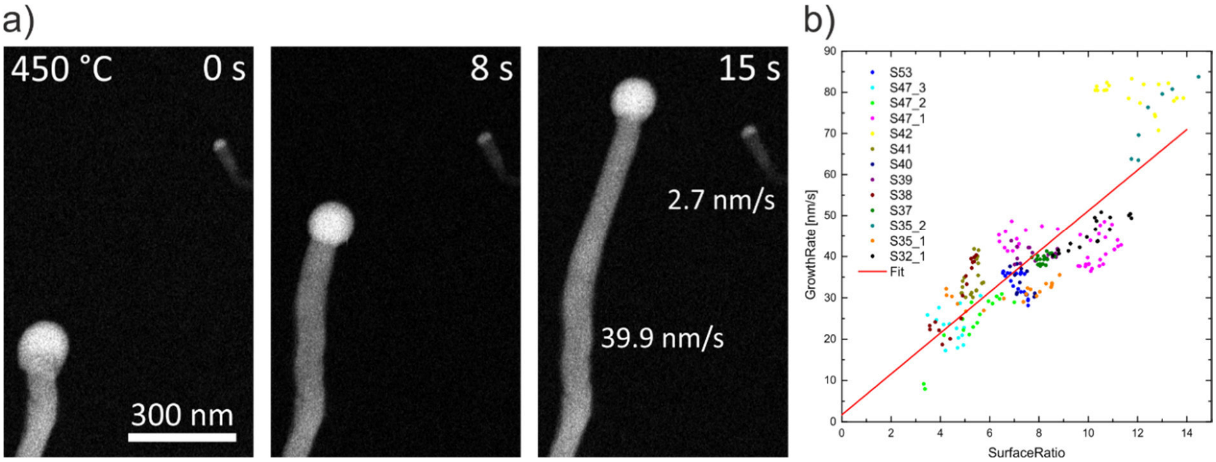

Fig. 2 a) STEM images of two growing NWs. The deviating surface ratios lead to different growth rates. b) Growth rate measurements of 13 NWs in dependence of their surface ratio. Each color represents a single NW.

Teilnehmer GRK-Seminar

vom 21.09. - 23.09.2020
Kloster Höchst / Höchst im Odenwald

Adamkiewicz	Alexa
Bergmeier	Tim
Dunaj	Tobias
Glowatzki	Johannes
Günkel	Robin
Haust	Johannes
Hepp	Thilo
Kreuter	Florian
Kröner	Marcel
Liebscher	Sven Christian
Maßmeyer	Oliver
Mondal	Badal
Peters	Bertram
Pieck	Fabian
Ritter	Christian
Rost	Luise
Veletas	Julian
Widemann	Maximilian
Wilhelm	Mikko

Chatterjee	Sangam	Prof. Dr.
Dürr	Michael	Prof. Dr.
von Hänisch	Carsten	Prof. Dr.
Mette	Gerson	Dr.
Tonner	Ralf	Prof. Dr.
Volz	Kerstin	Prof. Dr.

Hier findet der Workshop statt:

Kloster Höchst
Jugendbildungsstätte und Tagungshaus der EKHN
Kirchberg 3
64739 Höchst im Odenwald
E-Mail: info@kloster-hoechst.de
Telefon: (06163) 9330-0
Fax: (06163) 9330-19

Lage

Südlich von Frankfurt/Main liegt Höchst im Odenwald im Bundesland Hessen, an der Grenze zu Bayern. Umgeben von der Burg Breuberg und der Veste Otzberg liegt das Tagungshaus inmitten der reizvollen Landschaft des hessischen Odenwaldes.

Sie erreichen das Kloster Höchst …

… mit dem PKW

Das Tagungshaus liegt mitten im Grünen und doch verkehrsgünstig und zentral. Mit dem Auto oder der Odenwaldbahn erreichen Sie das Kloster Höchst von Frankfurt am Main aus in weniger als einer Stunde.

Für Anreisende mit dem PKW befindet sich ein ausgeschilderter Gästeparkplatz in der Frankfurter Straße 16.

… mit öffentlichen Verkehrsmitteln

Bahnreisende fahren einfach bis Bahnhof Höchst/Odw. Der Fußweg von dort zum Kloster beträgt ca. 10 Minuten.

Nach Verlassen des Bahnhofs laufen Sie die Bahnhofstraße bergab. An der unteren Weggabelung wenden Sie sich nach links, überqueren an der Ampel die Hauptstraße und gehen geradeaus bis zum Kirchberg. Vor der Sparkasse biegen Sie links zum Kloster ein.